

1 **COVID-19 lockdown induced changes in NO₂ levels across India observed**
2 **by multi-satellite and surface observations**

3 Akash Biswal^{1,2}, Vikas Singh^{1*}, Shweta Singh¹, Amit P. Kesarkar¹, Khaiwal Ravindra³,
4 Ranjeet S. Sokhi⁴, Martyn P. Chipperfield^{5,6}, Sandip S. Dhomse^{5,6}, Richard J. Pope^{5,6},
5 Tanbir Singh², Suman Mor²

6
7 1. National Atmospheric Research Laboratory, Gadanki, AP, India

8 2. Department of Environment Studies, Panjab University, Chandigarh 160014, India

9 3. Department of Community Medicine and School of Public Health, Post Graduate Institute
10 of Medical Education and Research (PGIMER), Chandigarh 160012, India

11 4. Centre for Atmospheric and Climate Physics Research (CACR), University of Hertfordshire,
12 Hatfield, UK

13 5. School of Earth and Environment, University of Leeds, Leeds, UK

14 6. National Centre for Earth Observation, University of Leeds, Leeds, UK

15 **Correspondence to: Vikas Singh (vikas@narl.gov.in)*

16 **Abstract**

17 We have estimated the spatial changes in NO₂ levels over different regions of India during the
18 COVID-19 lockdown (25th March – 3rd May 2020) using the satellite-based tropospheric
19 column NO₂ observed by the Ozone Monitoring Instrument (OMI) and the Tropospheric
20 Monitoring Instrument (TROPOMI), as well as surface NO₂ concentrations obtained from the
21 Central Pollution Control Board (CPCB) monitoring network. A substantial reduction in NO₂
22 levels was observed across India during the lockdown compared to the same period during
23 previous business-as-usual years, except for some regions that were influenced by anomalous
24 fires in 2020. The reduction (negative change) over the urban agglomerations was substantial
25 (~20-40 %) and directly proportional to the urban size and population density. Rural regions
26 across India also experienced lower NO₂ values by ~15-25 %. Localised enhancements in NO₂
27 associated with isolated emission increase scattered across India were also detected. Observed
28 percentage changes in satellite and surface observations were consistent across most regions
29 and cities, but the surface observations were subject to larger variability depending on their

30 proximity to the local emission sources. Observations also indicate NO₂ enhancements of up
31 to ~ 25 % during the lockdown associated with fire emissions over the north-east of India, and
32 some parts of the central regions. Besides, the cities located near the large fire emission sources
33 show much smaller NO₂ reduction than other urban areas as the decrease at the surface was
34 masked by enhancement in NO₂ due to the transport of the fire emissions.

35 **Keywords:** OMI, TROPOMI, CPCB, Emission reduction, Air quality, ISRO LULC

36 **1 Introduction**

37 Nitrogen oxides NO_x (NO+NO₂) are one of the major air pollutants, as defined by various
38 national environmental agencies across the world, due to their adverse impact on human health
39 (Mills et al., 2015). Furthermore, tropospheric levels of NO_x can affect tropospheric ozone
40 formation (Monks et al., 2015), contribute to the secondary aerosol formation (Lane et al.,
41 2008), acid deposition, and impact climatic cycles (Lin et al., 2015). The major anthropogenic
42 sources of NO_x emissions include the combustion of fossil fuels in road transport, aviation,
43 shipping, industries, and thermal power plants (e.g., USEPA, 1999; Ghude et al., 2013; Hilboll
44 et al., 2017). Other sources include open biomass burning (OBB), mainly large-scale forest
45 fires (e.g., Hilboll et al., 2017), lightning (e.g., Solomon et al., 2007) and emissions from soil
46 (e.g., Ghude et al., 2010). NO_x hotspots are often observed over regions with large thermal
47 power plants, industries as well as urban areas with significant traffic volumes causing large
48 localised emissions (e.g., Prasad et al., 2012; Hilboll et al., 2013; Ghude et al., 2013).

49 With growing scientific awareness of the adverse impacts of air pollution, the number of air
50 quality monitoring stations has expanded to over 10,000 across the globe (Venter et al., 2020).
51 Additionally, multiple satellite instruments such as the Global Ozone Monitoring Instrument
52 (GOME) on ERS-2, the Scanning Imaging Absorption Spectrometer for Atmospheric
53 Cartography (SCIAMACHY, 2002-2012) on Envisat, the Ozone Monitoring Instrument (OMI,
54 2005-present) on Aura, GOME-2 (2007-present) on MetOp and the TROPOspheric Monitoring
55 Instrument (TROPOMI, 2017-present) on Sentinel-5P (S5P) have monitored NO₂ pollution
56 from the space for over two decades. Surface sites typically measure NO₂ in concentration
57 quantities (e.g., µg m⁻³), but satellite NO₂ measurements are retrieved as integrated vertical
58 columns (e.g., tropospheric vertical column density, VCD_{trop}). The latter is preferred for
59 studying NO₂ trends and variabilities because of global spatial coverage and spatio-temporal
60 coincidence with ground-based measurements (Martin et al., 2006; Kramer et al., 2008; Lamsal
61 et al., 2010; Ghude et al., 2011). NO₂ has been reported to increase in south Asian countries

62 (Duncan et al., 2016; Hilboll et al., 2017; ul-Haq et al., 2017), decrease over Europe (van der
63 A et al., 2008; Curier et al., 2014; Georgoulas et al., 2019) and the United States (Russell et
64 al., 2012; Lamsal et al., 2015). In the case of India, a tropospheric NO₂ increase was observed
65 during the 2000s (e.g., Mahajan et al., 2015), but since 2012 it has either stabilized or even
66 declined owing to the combined effect of economic slowdown and adoption of cleaner
67 technology (e.g., Hilboll et al., 2017). However, thermal power plants, megacities, large urban
68 areas and industrial regions remain NO₂ emission hotspots (Ghude et al., 2008, 2013; Prasad
69 et al., 2012; Hilboll et al., 2013, 2017; Duncan et al., 2016;). Moreover, despite the measures
70 taken to control NO_x emissions, urban areas often exceed national ambient air quality standards
71 in India (Sharma et al., 2013; Nori-Sarma et al., 2020; Hama et al., 2020), and thus require a
72 detailed scenario analysis.

73 The nationwide lockdown in various countries during March-May 2020, due to the outbreak
74 of COVID-19, reduced the traffic and industrial activities leading to a significant reduction of
75 NO₂. Studies using space-based and surface observations of NO₂ have reported reductions in
76 the range of ~30-60 % for China, South Korea, Malaysia, Western Europe, and the U.S.
77 (Bauwens et al., 2020; Kanniah et al., 2020; Muhammad et al., 2020; Tobías et al., 2020;
78 Dutheil et al., 2020; Liu et al., 2020; Huang and Sun 2020; Naeger and Murphy 2020; Barré et
79 al., 2020; Goldberg et al., 2020) against the same period in previous years, with the observed
80 reductions strongly linked to the restrictions imposed on vehicular movement. The lockdown
81 in India was implemented in various phases starting on the 25th March 2020 (MHA, 2020;
82 Singh et al., 2020). The lockdown restrictions in the first two phases (Phase 1: 25th March -
83 14th April 2020 and Phase 2: 15th April - 3rd May 2020) were the strictest, during which all non-
84 essential services and offices were closed and the movement of the people was restricted,
85 resulting in a considerable reduction in the anthropogenic emissions. The restrictions were
86 relaxed in a phased manner from the third phase onwards in less affected areas by permitting
87 activities and partial movement of people (MHA, 2020).

88 A decline in NO₂ levels over India during the lockdown has been reported from both surface
89 observations (Singh et al., 2020; Sharma et al., 2020; Mahato et al., 2020), as well as satellite
90 observations (ESA, 2020; Biswal et al., 2020; Siddiqui et al., 2020; Pathakoti et al., 2020)
91 against the previous year or average of few previous years. A detailed study by Singh et al.
92 (2020) based on 134 sites across India reported a decline of ~30–70 % in NO₂ during lockdown
93 with respect to the mean of 2017-2019, with a largest reduction being observed during peak
94 morning traffic hours and late evening hours. While Sharma et al. (2020) reported a smaller

95 decrease (18 %) in NO₂ for selected sites against the levels during 2017-2019, Mahato et al.
96 (2020) found a decrease of over 50 % in Delhi for the first phase of lockdown against previous
97 years (2017-2019), which was also confirmed by Singh et al. (2020) for the extended period of
98 analysis. The satellite-based studies by Biswal et al. (2020) and Pathakoti et al. (2020)
99 estimated the change in NO₂ levels using OMI observations, whereas Siddiqui et al. (2020)
100 used TROPOMI to compute the change over eight major urban centres of India. Biswal et al.
101 (2020) reported that the average OMI NO₂ over India decreased by 12.7 %, 13.7 %, 15.9 %, and
102 6.1 % during the subsequent weeks of the lockdown relative to similar periods in 2019.
103 Similarly, Pathakoti et al. (2020) reported a decrease of 17 % in average OMI NO₂ over India
104 compared to the pre-lockdown period and a decrease of 18 % against the previous 5-year
105 average. Moreover, both studies reported a larger reduction of more than 50 % over Delhi.
106 Similarly, Siddiqui et al. (2020) also reported an average reduction of 46 % in the eight cities
107 during the first lockdown phase with respect to the pre-lockdown phase. While recent studies
108 have used either only satellite observations or only surface observations, this study goes further
109 by adopting an integrated approach by combining both measurement types to investigate NO₂
110 level changes over India in response to the COVID-19 pandemic using OMI, TROPOMI and
111 surface observations over different regions. As both OMI and TROPOMI have similar local
112 overpass times of approximately 13:30 (Penn and Holloway, 2020; van Geffen et al., 2020),
113 diurnal influences on the retrievals of NO₂ for both instruments are similar. Moreover, as both
114 instruments use nearly similar retrieval schemes (i.e., differential optical absorption
115 spectroscopy, DOAS), their NO₂ measurements are believed to be comparable with a suitable
116 degree of confidence (van Geffen et al., 2020; Wang et al., 2020). Any product differences are
117 likely to be caused by inconsistent inputs/processing of the retrievals (e.g., derivation of the
118 stratospheric slant column, the a priori tropospheric NO₂ profile and the treatment of
119 aerosols/clouds in the calculation of the air mass factor (van Geffen et al., 2019; Lasmal et al.,
120 2021)).

121 We estimate the changes in the NO₂ levels over different land-use categories (i.e., urban,
122 cropland and forestland) and urban sizes. In addition to this, we investigate the spatial
123 agreement between population density and NO₂ spatial variability observed at the surface. A
124 key benefit of this study will be to understand and assess the impact of reduced anthropogenic
125 activity on NO₂ levels not only over the urban areas but also over the rural areas (cropland and
126 forestland). This study thus provides an improved understanding of the spatial variations of
127 tropospheric NO₂ for future air quality management in India.

128 **2 Data and methodology**

129 **2.1 Data**

130 Satellite observations of $VCD_{trop} NO_2$ were obtained from OMI (2016-2020) and TROPOMI
131 (2019-2020). Surface NO_2 observations (2016-2020) at 139 sites across India were from the
132 Central Pollution Control Board (CPCB). The period from 25th March to 3rd May each year is
133 defined as the analysis period. Average NO_2 levels during the analysis period in 2020 and
134 previous years are referred to as lockdown (LDN) NO_2 and business as usual (BAU) NO_2 ,
135 respectively. The BAU years for OMI and CPCB are 2016-2019, whereas for TROPOMI the
136 BAU year is 2019 because of the unavailability of earlier observations.

137 NO_2 data were analysed for six geographical regions (north, Indo Gangetic Plain (IGP), north-
138 west, north-east, central and south) of India (supplementary Fig. S1). The NO_2 changes over
139 various land-use categories (i.e., urban, cropland and forestland) have been analysed using
140 spatially collocated land-use land cover (LULC) data (NRSC, 2012) and OMI and TROPOMI
141 observed $VCD_{trop} NO_2$. Visible Infrared Imaging Radiometer Suite (VIIRS) fire count data was
142 used to study the fire anomalies during the LDN and other analysis periods.

143 **2.1.1 OMI NO_2**

144 OMI has a nadir footprint of approximately $13 \text{ km} \times 24 \text{ km}$, measuring in the ultraviolet-visible
145 (UV-Vis) spectral range of 270-500 nm (Boersma et al., 2011). It uses differential optical
146 absorption spectroscopy (DOAS) to retrieve VCD_{trop} (i.e., VCD_{trop} is the difference between
147 the total and stratospheric slant columns divided by the tropospheric air mass factor (Boersma
148 et al., 2004)). Here, we use the OMI NO_2 30 % Cloud-Screened Tropospheric Column L3
149 Global Gridded (Version 4) at a $0.25^\circ \times 0.25^\circ$ ($\sim 25 \text{ km} \times 25 \text{ km}$) spatial grid from the NASA
150 Goddard Earth Sciences Data and Information Services Center (GESDISC) available at
151 (https://disc.gsfc.nasa.gov/datasets/OMNO2d_003/summary). Details of the retrieval scheme
152 and OMI data product Version 4 are discussed by Krotkov et al., (2019) and Lamsal et al.,
153 (2021) and for older versions by e.g., Celarier et al. (2008) and Krotkov et al. (2017).

154 **2.1.2 TROPOMI NO_2**

155 TROPOMI has a nadir-viewing spectral range of 270–500 nm (UV-Vis), 675–775 nm (near-
156 infrared, NIR) and 2305–2385 nm (short wave-infrared, SWIR). In the UV-Vis and NIR
157 wavelengths, TROPOMI has an unparalleled spatial footprint of $3.5 \text{ km} \times 7.0 \text{ km}$, along with
158 $7 \text{ km} \times 7 \text{ km}$ in the SWIR (Veefkind et al., 2012). Details of the TROPOMI scheme and data
159 are discussed by Eskes et al. (2019) and Van Geffen et al. (2019). The TROPOMI $VCD_{trop} NO_2$

160 over India for the analysis period was obtained at 3.5 km × 7 km resolution from
161 (<http://www.temis.nl/airpollution/no2.php>) and re-gridded at a spatial resolution of 0.05° ×
162 0.05° (~ 5 km × 5 km) based on the gridding methodology of Pope et al. (2018). The source
163 data are filtered to remove pixels with QA (Quality Assurance) values greater than 50, which
164 removes cloud fraction less than 0.2, part of the scenes covered by snow/ice, errors and
165 problematic retrievals (Eskes et al., 2019).

166 Although substantial differences are found between OMI and TROPOMI (such as the
167 differences in the orbit and spatial resolution, van Geffen et al., 2020), they exhibit good
168 correlation with the surface observations (Chan et al., 2020; Wang et al., 2020) but are ~ 30 %
169 lower than the Multi-axis differential optical absorption spectroscopy (MAX-DOAS)
170 observations. Overall, TROPOMI has been reported to be superior to OMI (van Geffen et al.,
171 2020). Detailed descriptions of the recent retrieval schemes used for TROPOMI and OMI data
172 products are provided in van Geffen et al. (2019) and Lamsal et al. (2021), respectively.
173 Analysis of differences between these two satellite data products is beyond the scope of this
174 study.

175

176 **2.1.3 Surface NO₂ concentration**

177 The hourly averaged surface NO₂ concentration at 139 sites (Fig. S1) for 2016-2020 across
178 India was acquired from the CPCB CAAQMS (Continuous Ambient Air Quality Monitoring
179 Stations) portal (<https://app.cpcbccr.com/ccr/#/caaqm-dashboard-all/caaqm-landing>). The data
180 was further quality controlled by removing the outliers, constant values, and sites with less than
181 60 % data during the analysis period. Details of the surface observations are explained in Singh
182 et al. (2020).

183 **2.1.4 Land use land cover data**

184 The high-resolution (50 m × 50 m) LULC data mapped with level-III classification for 18 major
185 categories (NRSC, 2012) was obtained from the BHUVAN geo-platform ([https://bhuvan-
186 app1.nrsc.gov.in/thematic/thematic/index.php](https://bhuvan-app1.nrsc.gov.in/thematic/thematic/index.php)) of the Indian Space Research Organisation
187 (ISRO). To quantify the changes over urban, crop and forest areas, the OMI and TROPOMI
188 NO₂ at urban grids (category 1), cropland (category 2 to 5) and forestland (category 7 to 10)
189 were extracted for further analysis. In order to match the OMI and TROPOMI grid resolution
190 with the Indian LULC, the dominant LULC was considered within the OMI and TROPOMI
191 grid. Supplementary Fig. S2 shows the high-resolution LULC data used in this study for

192 cropland, forestland, and urban areas separately. Urban areas were further divided into four
193 sizes (10-50 km², 50-100 km², 100-200 km² and greater than 200 km²) to study the change in
194 NO₂ with respect to the size of the urban agglomeration.

195 **2.1.5 VIIRS fire counts**

196 The VIIRS aboard the Suomi National Polar-orbiting Partnership (S-NPP) satellite provides
197 daily global fire count at a 375 m × 375 m spatial resolution (Schroeder et al., 2014; Li et al.,
198 2018). The fire count data over India during the analysis period from 2016 to 2020 was obtained
199 from the FIRMS (Fire Information for Resource Management System) web portal
200 (<https://firms.modaps.eosdis.nasa.gov/download/>). The fire count data was gridded at 5 km ×
201 5 km for each year by summing the fire counts falling on each spatially overlapping grid. The
202 burnt area was calculated from the fire counts by multiplying with the VIIRS grid size (Prosperi
203 et al., 2020).

204 **2.1.6 Population data**

205 The gridded population density (people per hectare, pph) data for 2020 was taken from
206 Worldpop (2017). Worldpop estimates the population density at approximately 100 m × 100 m
207 (near the equator) by disaggregating census data for population mapping using random forest
208 estimation technique using remotely sensed and ancillary data. Details of the population
209 mapping methodology can be found in Stevens et al. (2015).

210 **2.1.7 Google mobility change**

211 Google estimated the change in the people movement from 15th February 2020 onwards based
212 on the Google maps information of people's location at retail & recreation, grocery &
213 pharmacy, parks, transit stations, workplaces, and residential places etc. The changes were
214 estimated with reference to the baseline days that represent a normal value for that day of the
215 week. The baseline day is the median value from the five-week period Jan 3 – Feb 6, 2020.
216 The google mobility change dataset provided an excellent proxy for the anthropogenic activity
217 change and has therefore been used for several purposes of air quality studies such as lockdown
218 emission estimation and temporal relation with pollutant species (Archer et al., 2020; Forster
219 et al., 2020; Gama et al., 2020; Guevara et al., 2021) during the lockdown period of 2020. The
220 Google mobility data and reports are available at (<https://www.google.com/covid19/mobility>).

221 **2.1.8 Meteorological data**

222 The Copernicus Climate Change Service (C3S) provides the ERA5 reanalysis (Hersbach et al.,
223 2020) meteorological data with an improved vertical, temporal and spatial coverage. The

224 monthly mean meteorological data (temperature, wind speed and planetary boundary layer
225 height) at $0.25^\circ \times 0.25^\circ$ resolution for March, April and May of 2016-2020 were used for the
226 analysis. For details, see <https://www.ecmwf.int/en/forecasts/datasets/reanalysis-datasets/era5>
227 (last access: 25 January 2021).

228 **2.1.9 Analysis methodology**

229 The change in the NO₂ levels for each analysis period has been calculated by subtracting the
230 BAU NO₂ from LDN NO₂. We calculate the percentage change (D) using the equation

$$231 \quad D = \frac{(LDN - BAU)}{BAU} \times 100$$

232 The analysis was done over the whole of India as well as over the separate considered regions
233 and selected LULC categories using the open-source Geographic Information System (QGIS).

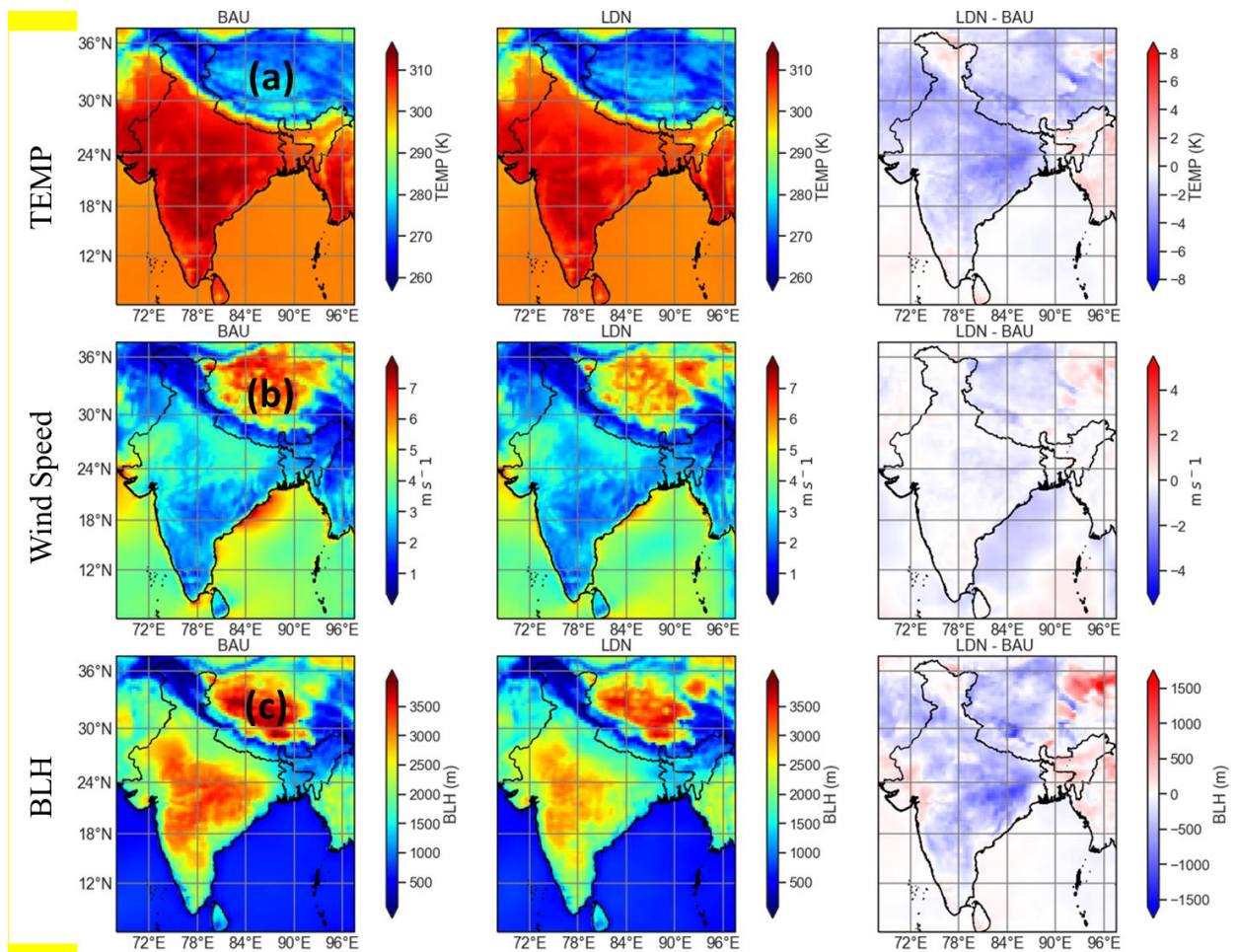
234 **3 Results and Discussion**

235 **3.1 Meteorological variations**

236 Air pollutant concentration over a region is governed by emission sources and prevailing
237 meteorological conditions. Meteorological factors (e.g., wind, temperature, radiation rainfall
238 etc) can affect the NO₂ concentration (Barré et al., 2020) as well as biogenic emissions
239 (Guenther et al., 2012). The meteorological variations between years can cause ~ 15 %
240 variations in monthly column NO₂ values (Goldberg et al., 2020). However, the NO₂ levels are
241 likely to be similar under similar meteorological conditions. Recent studies (e.g., Singh et al.,
242 2020; Navinya et al., 2020; Sharma et al., 2020) have shown that meteorological conditions
243 remained relatively consistent over recent years during the lockdown period and therefore
244 assumed that the changes in the pollution levels during the lockdown are primarily driven by
245 the emission changes. However, it is important to highlight the meteorological differences
246 during the study period to assess the uncertainties associated with meteorological differences.

247 We used monthly mean ERA-5 reanalysis data (Hersbach et al., 2020) at $0.25^\circ \times 0.25^\circ$
248 resolution for March, April and May for BAU as well as LDN periods at the satellite local
249 overpass time. We considered temperature (T), wind speed (WS) and boundary layer height
250 (BLH) in our analysis. Fig. 1 (a-c) shows the spatial variation in these quantities during BAU
251 (left panel), LDN (middle panel) and the calculated difference (LDN-BAU, right-panel). The
252 probability density function (PDF) using kernel density estimation (KDE) of the
253 meteorological parameters are also shown (Fig. S3) for the BAU (blue) and LDN (red). KDE

254 is a non-parametric way to estimate the PDF. The peak of the distribution shows the most
255 probable value, and the width of the distribution shows the variability. The temperature
256 difference between LDN and BAU shows a slight reduction (~0-3 K range) during the
257 lockdown. Wind speed values also show a reduction (up to 2 ms⁻¹) during the lockdown,
258 although the reduction is mainly seen in certain parts of central India. Reduction in the BLH is
259 also seen in most parts of India. In general, the meteorological parameters during the lockdown
260 were similar. However, the PDF (Fig. S3) during BAU and LDN show a small reduction (less
261 than 5 %) in temperature and wind speed and ~ 10 % reduction in BLH. Although small, this
262 weather variability can further add to the variability in the NO₂ levels. However, during the
263 lockdown in India, the NO₂ change was more sensitive to the emission change than the
264 meteorology variability. Shi et al. (2021) compared the detrended and de-weathered change in
265 NO₂ observed over selected cities from India, Europe, China and USA. While the reduction in
266 NO₂ was highest for Delhi (~50%), the difference between a detrended and de-weathered
267 change in NO₂ observed over Delhi was much smaller (~2%) as compared to the difference
268 calculated for other cities. This suggests that weather variability did not have much impact on
269 NO₂ levels over India and most of the changes were driven by a change in the anthropogenic
270 emissions.



271

272 *Fig. 1: Spatial map showing the variation in surface meteorological parameters (a.*
 273 *temperature, b. wind speed and c. BLH) from ERA-5 by comparing BAU (left column), LDN*
 274 *(middle) and observed difference (LDN-BAU, right).*

275

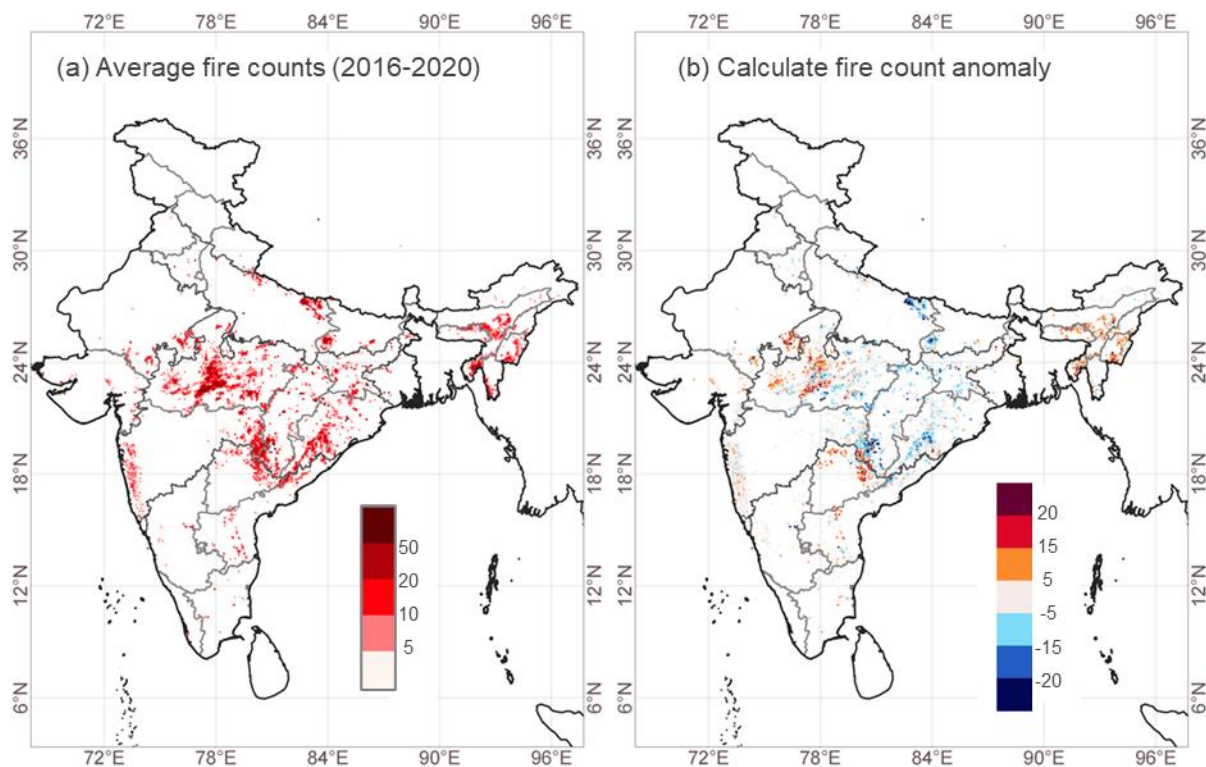
276 3.2 Fire count anomalies during the lockdown

277 Forest fires are an important source of surface NO_2 and VCDtrop NO_2 (Sahu et al., 2015;
 278 Yarragunta et al., 2020), depending on the occurrence time and the intensity of fires (Mebust
 279 et al., 2011). Also, as the forest fire plumes can be transported longer distances (Alonso-Blanco
 280 et al., 2018), forest-fire-related NO_2 can contribute to regional and global air pollution. In India,
 281 forest fires are prevalent as 36 % of the country's forest cover is prone to frequent fires, out of
 282 which nearly 10 % is extremely to very highly prone to fires (ISFR 2019). Long-term satellite-
 283 derived fire counts suggest that Indian fire activities typically peak during March-May (Sahu
 284 et al., 2015), predominantly over the north, central and north-east regions (Venkataraman et
 285 al., 2006; Ghude et al., 2013). However, the spatial and temporal distribution of fire events is

286 largely heterogeneous (Sahu et al., 2015), meaning an abrupt increase or decrease in fire
287 activity could significantly impact NO₂ levels over anomalous regions during the lockdown.

288 An investigation of fire counts during the 2020 lockdown (LDN analysis period), when
289 compared with the corresponding 2016-2020 average, highlights a substantial decrease over
290 the eastern part of central India and an increase over the western part of central India and north-
291 east. In Fig. 2a widespread fire activity (counts of 10-50) is shown across India, such as the
292 central region (Madhya Pradesh, Chhattisgarh, Odisha), parts of Andhra Pradesh, the Western
293 Ghats in Maharashtra and the north-east region (Assam, Meghalaya, Tripura, Mizoram and
294 Manipur). The fire anomaly during the lockdown (Fig. 2b) shows positive fire counts (5-20)
295 over the north-east region, west of Madhya Pradesh in central India and scattered locations in
296 South India. The negative fire anomalies (-20 to -5) observed over the central region
297 (Chhattisgarh and Odisha) suggests a decrease in fire activity during the 2020 lockdown period.
298 To minimise the impact of fire emission in our analysis, we have considered the grids with zero
299 fire anomaly to assess the changes in NO₂ during the lockdown. By considering the grids with
300 zero fire anomaly, we excluded almost all the grids which have recorded fire activity during
301 the analysis period. However, the impact of long-range transport of forest fire plumes cannot
302 be ignored.

303

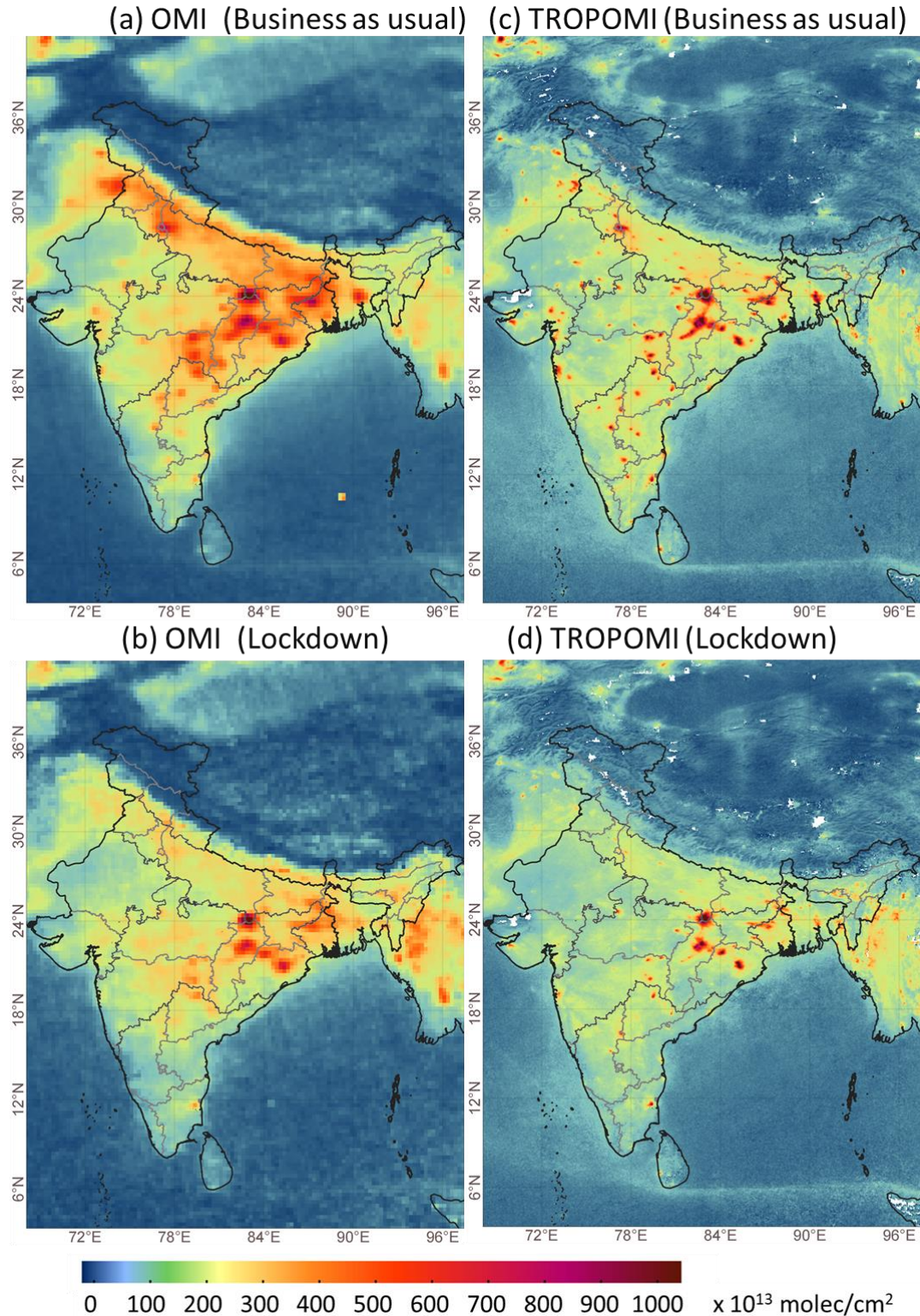


304

305 *Fig. 2* Spatial distribution of the **5 km × 5 km gridded** VIIRS fire counts. (a) Average fire
 306 counts during the analysis period (March 25th - May 3rd, 2016-2020). (b) Gridded fire
 307 anomaly during the lockdown in 2020.

308 3.3 VCD_{trop} NO₂ over India during lockdown period

309 The spatial distribution of VCD_{trop} NO₂ is largely determined by local emission sources;
 310 **therefore**, NO₂ hotspots are found over urban regions, thermal power plants and major
 311 industrial corridors. For the Indian subcontinent, maximum NO₂ is observed during winter to
 312 pre-monsoon (Dec-May) and minimum NO₂ during the monsoon (Jun-Sep). Region-specific
 313 peaks such as the winter-time peak (Dec-Jan) in the IGP is associated with anthropogenic
 314 emissions, or the summer-time peak (Mar-Apr) in central India and north-east India is
 315 associated with enhanced biomass burning activities (Ghude et al., 2008; Ghude et al., 2013;
 316 Hilboll et al., 2017).



317

318 **Fig. 3** Spatial distribution of mean $VCD_{trop} NO_2$ (molecules cm^{-2}) during the analysis period
 319 (25th March - 3rd May) for (a) OMI NO_2 during business as usual (BAU, 2016-2019), (b) OMI
 320 NO_2 during the lockdown (LDN, 2020), (c) TROPOMI NO_2 during BAU (2019) and, (d)
 321 TROPOMI NO_2 during LDN (2020).

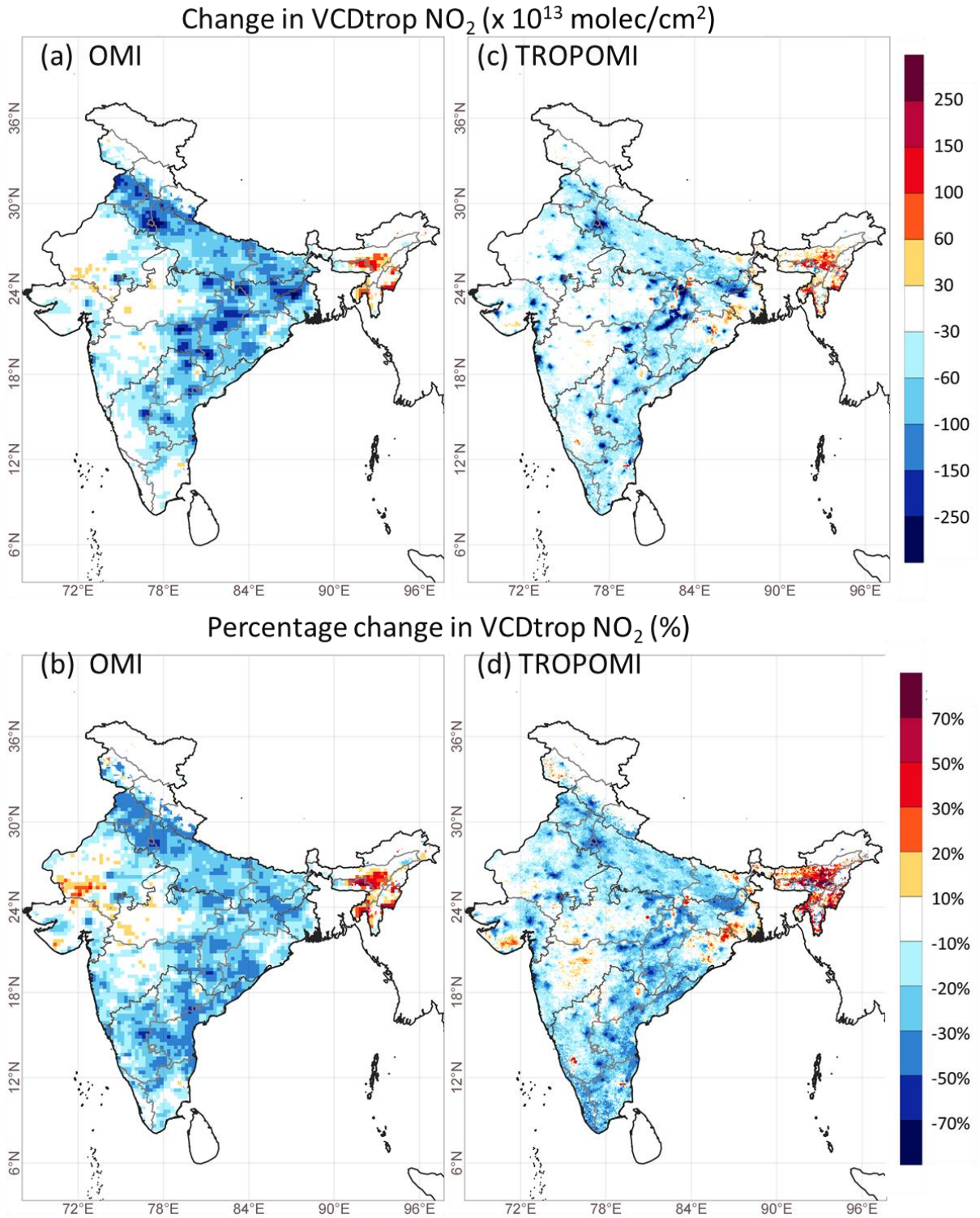
322 We compare the LDN mean $VCD_{trop} NO_2$ with the BAU mean for OMI and TROPOMI. The
323 spatial distribution of the BAU and LDN $VCD_{trop} NO_2$ observed by OMI and TROPOMI is
324 shown in Fig. 3 (a-d). The mean $VCD_{trop} NO_2$ from the two instruments shows similar spatial
325 distributions during the LND and BAU analysis period. In BAU years, the NO_2 hotspots are
326 seen over the large fossil-fuel-based thermal power plants ($\sim 1000 \times 10^{13}$ molecules cm^{-2}), urban
327 areas ($\sim 400-700 \times 10^{13}$ molecules cm^{-2}) and industrial areas. Scattered sources are also present
328 in western India, covering the industrial corridor of Gujarat and Mumbai, various locations of
329 south India, and densely populated areas (e.g., IGP). The spatial distribution showed significant
330 changes during the lockdown in 2020. The details of actual and percentage changes are
331 discussed in the subsequent sections.

332 3.4 Changes observed by OMI and TROPOMI

333 There is a substantial reduction in $VCD_{trop} NO_2$ between the LDN and BAU (Fig. 4a & c). A
334 large reduction in the number of hotspots, mainly urban areas, is seen in both OMI and
335 TROPOMI observations. However, hotspots due to coal-based power plants remain during the
336 lockdown as electricity production was continued. Over the NO_2 hotspots, there has been an
337 absolute decrease of over 150×10^{13} molecules cm^{-2} ($\sim 250 \times 10^{13}$ molecules cm^{-2} over
338 megacities) detected by both OMI and TROPOMI. The rural $VCD_{trop} NO_2$ has typically
339 reduced by approximately $30-100 \times 10^{13}$ molecules cm^{-2} , representing a percentage decrease of
340 30-50 % for OMI and 20-30 % for TROPOMI (Fig. 4b & d). For urban regions, both OMI and
341 TROPOMI see a decrease of approximately 50 %, but reductions in smaller urban areas are
342 clearly noticeable in the TROPOMI data, given its better spatial resolution. Both instruments
343 observe an increase in $VCD_{trop} NO_2$ in the north-eastern regions and moderate enhancement
344 over the western and central regions. These enhancements are linked with the biomass burning
345 activities during this period (Fig. 2).

346

347



348

349 **Fig. 4** (a, c) Absolute change and (b, d) percentage change in VCD_{trop} NO₂ during the analysis
 350 period for LDN year compared to BAU years as observed by OMI (left panels) and TROPOMI
 351 (right panels).

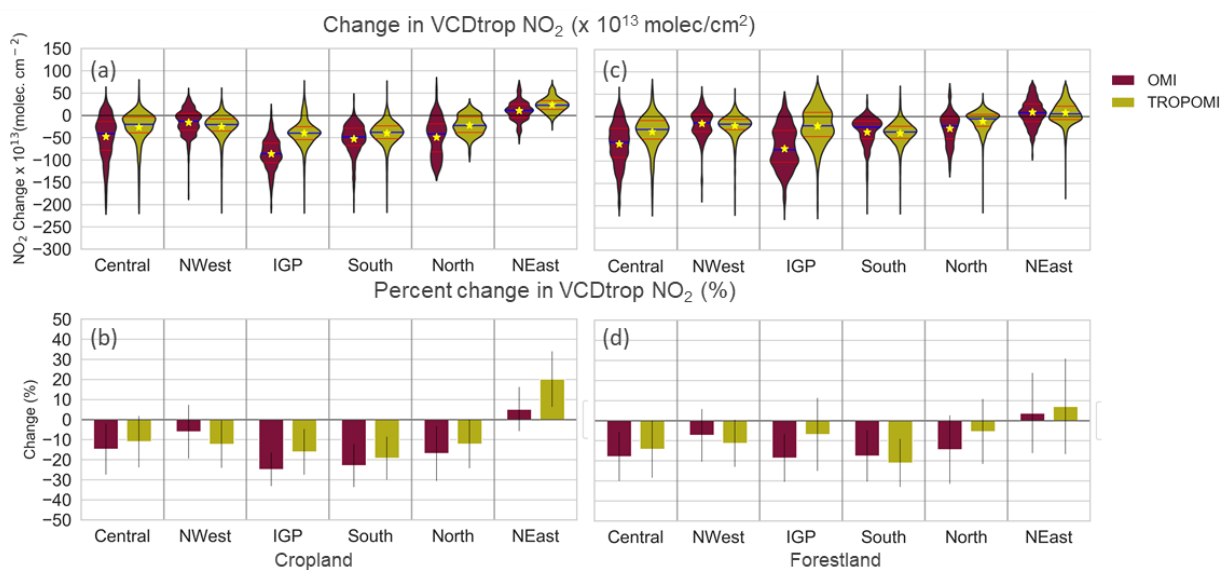
352

353 3.5 Changes in NO₂ over different land use types

354 Anthropogenic NO_x emissions are typically more localised in urban and industrial centres,
355 while biogenic sources (e.g., soil) are more important in rural regions. OBB activities peak in
356 March-April (Sahu et al., 2015) and represent more sporadic sources. As the lockdown is
357 expected to have reduced urban anthropogenic NO_x sources (as shown in Fig. 4), it is important
358 to assess the lockdown impact over the rural regions such as cropland and forestland as well.
359 This section estimates the changes in VCD_{trop} NO₂ over different land-types such as cropland,
360 forestland, and urban areas (Fig. S2). Industrial emissions are often part of the urban
361 agglomerates scattered around the city and are part of urban emissions. To minimise the impact
362 of OBB emissions in our analysis, we exclude grids with fire anomalies (Fig. 2) and those
363 containing thermal power plants (Fig. S2d). However, absolute separation of the impact of the
364 long-range transportation is beyond the scope of this study.

365 3.5.1 Changes over cropland and forestland

366 The changes in VCD_{trop} NO₂ observed by OMI and TROPOMI over the cropland (Fig. S2a) in
367 different regions of India are shown in Fig. 5a & b and Table S1. A decline in VCD_{trop} NO₂ has
368 been observed over croplands in all regions except for the north-east. A higher percentage
369 decline was observed over IGP and south regions by both the satellites. While VCD_{trop} NO₂
370 has decreased, prominent enhancements have been observed over the north-east and few grids
371 in central and north-west regions. These enhancements can be attributed to the impact of nearby
372 forest fires (Fig. 2). The observed changes over the forestland (Fig. S2c) over different regions
373 of India have been shown in Fig. 5 c & d and Table S1. The average VCD_{trop} NO₂ has declined
374 over forestland in all the regions except for the north-east where VCD_{trop} NO₂ was enhanced
375 due to the positive fire anomaly (Fig. 2) during the analysis period. It can be noted that although
376 we have taken the grids with zero fire anomaly, the effect of a nearby grid exhibiting positive
377 fire anomaly cannot be ignored due to atmospheric dispersion and mixing. The inter-
378 comparison of the changes observed by two satellites suggests that OMI data indicates a larger
379 reduction in VCD_{trop} NO₂ than TROPOMI in most of the regions.



380

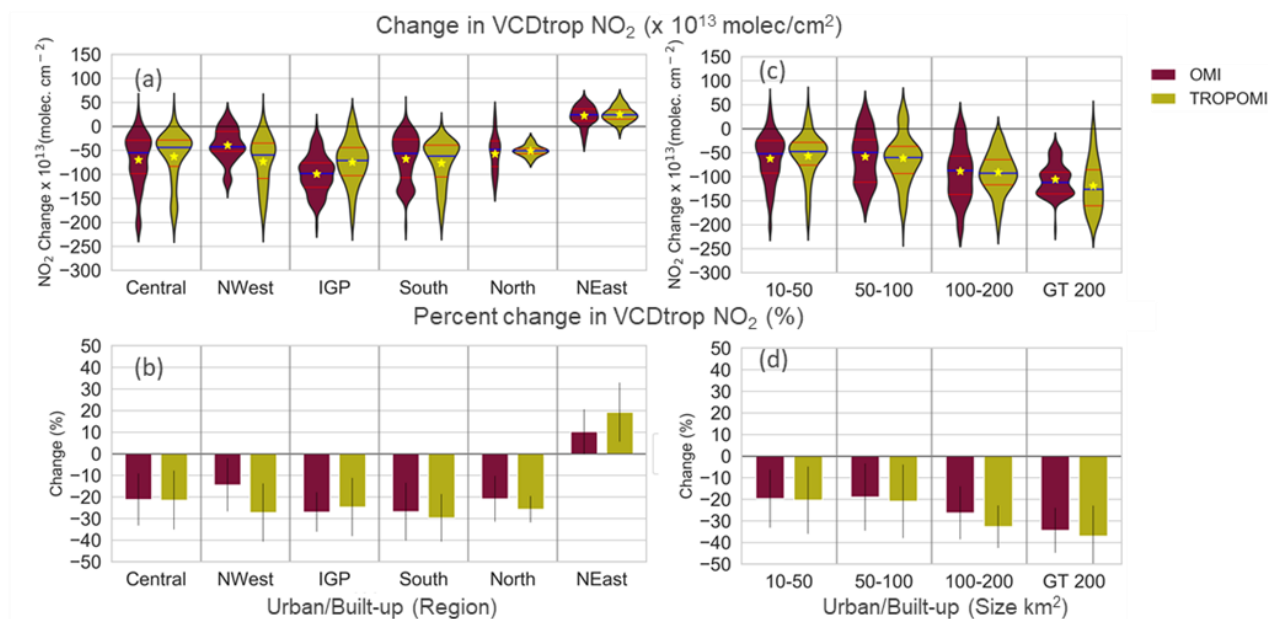
381

382 *Fig. 5* Observed change in $VCD_{trop} NO_2$ between LDN and BAU from OMI and TROPOMI for
 383 different regions shown as (a) violin plot of the absolute change over cropland, (b) percentage
 384 change over cropland, (c) violin plot of the absolute change over forestland, and (d) percentage
 385 change over forestland. A violin plot is a combination of a box plot and a kernel density
 386 estimation (KDE) plot. KDE is a non-parametric way to estimate the probability density
 387 function (PDF). The red lines in the violin plot show the interquartile range; the blue line
 388 shows the median value; the yellow star shows the mean value. The vertical lines in the bar
 389 plot show the standard deviation. The abbreviations NWest and NEast are for north-west and
 390 north-east regions, respectively.

391

392 3.5.2 Changes over urban regions

393 We analysed the changes in $VCD_{trop} NO_2$ over the urban areas (Fig. S2b) in different regions
 394 of India. The calculated actual and percentage changes observed by OMI and TROPOMI are
 395 shown in Fig. 6 and in Table S1. The mean changes observed by OMI and TROPOMI show
 396 similar variations in different regions. The changes observed over urban areas are larger than
 397 those observed over the forest and croplands. In contrast to the cropland and forestland,
 398 TROPOMI observed a larger reduction in $VCD_{trop} NO_2$ than OMI in most of the regions.
 399 Densely populated IGP with the largest urban agglomeration shows the maximum change in
 400 $VCD_{trop} NO_2$ followed by the central and north-west regions. The $VCD_{trop} NO_2$ over the urban
 401 areas in the north-east region is likely to be influenced by the nearby forest fires through
 402 atmospheric dispersion and mixing, resulting in the enhancement of $VCD_{trop} NO_2$ over the
 403 urban grids.



404

405 **Fig. 6** *Observed* change in VCD_{trop} NO₂ between LDN and BAU from OMI and TROPOMI for
 406 different regions shown as (a) Violin plot of the absolute change over urban areas, (b)
 407 percentage change over the urban area, (c) violin plot of the observed change over different
 408 sized urban areas, and (d) percentage change over different sized urban areas.

409 We have also analysed the change in the VCD_{trop} NO₂ over urban areas of different sizes. We
 410 have taken the urban areas of sizes more than 10 km² and grouped them into four bins of size
 411 10-50 km², 50-100 km², 100-200 km², and greater than 200 km². We then calculate the changes
 412 observed for all the cities filling into the respective bins. Fig. 6 (c & d) show the absolute and
 413 percentage change in VCD_{trop} NO₂, as observed by OMI and TROPOMI, respectively. A
 414 significant reduction of 50-150 × 10¹³ molecules cm⁻² (20-40 %) was observed over the urban
 415 area of different sizes. The actual reduction in VCD_{trop} NO₂ is greater for the larger urban area
 416 with peak reductions for the urban area bin (> 200 km²) for both OMI and TROPOMI. **The
 417 greater reduction in the larger urban areas is mainly due to the reduction in local emission
 418 sources, as evidenced by the Google mobility reduction, which is higher for larger cities than
 419 the smaller ones (Fig. S6).**

420 3.5.3 Changes over thermal power plants

421 Thermal power plants (TPPs) are the hotspots of NO₂ pollution. These are scattered across the
 422 nation, with a majority of them in Madhya Pradesh, Bihar, Uttar Pradesh, Odisha, Gujarat,
 423 Chattisgarh, West Bengal, and Tamil Nadu (Fig S2d). During the lockdown period, TPPs were
 424 still operated to fulfill the electricity demands. In this section, we analyse the changes observed
 425 over TPPs. The changes in VCD_{trop} NO₂ observed by OMI and TROPOMI over the TPPs are
 426 shown in Fig. S5. A decrease in mean VCD_{trop} NO₂ levels over TPPs has been observed that

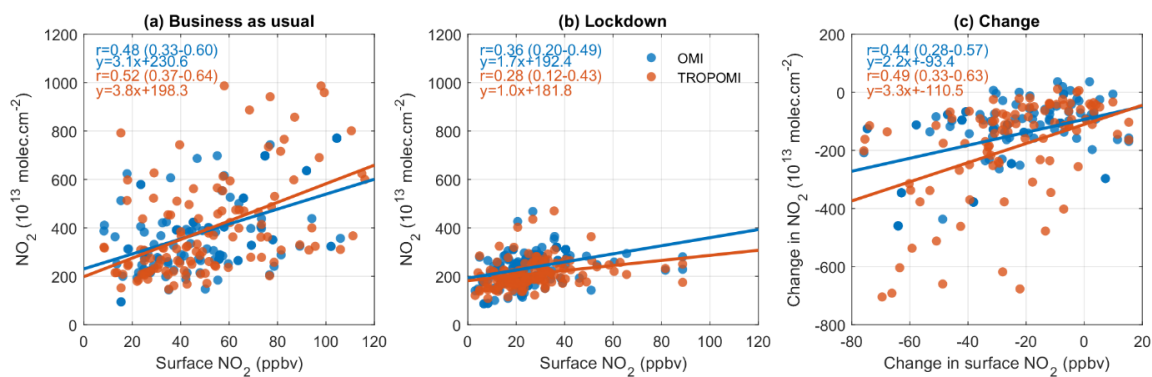
427 is in line with the power sector report, which mentions that during April 2020, energy demand
428 met for India decreased by 24 % as compared to April 2019 (POSOCO report:
429 <https://posoco.in/reports/monthly-reports/monthly-reports-2020-21/>). Also, there is a drop
430 (~30%) in thermal power production during the lockdown against to respective period of 2019.

431

432 **3.6 Inter-comparison of changes observed by OMI, TROPOMI and surface** 433 **observation**

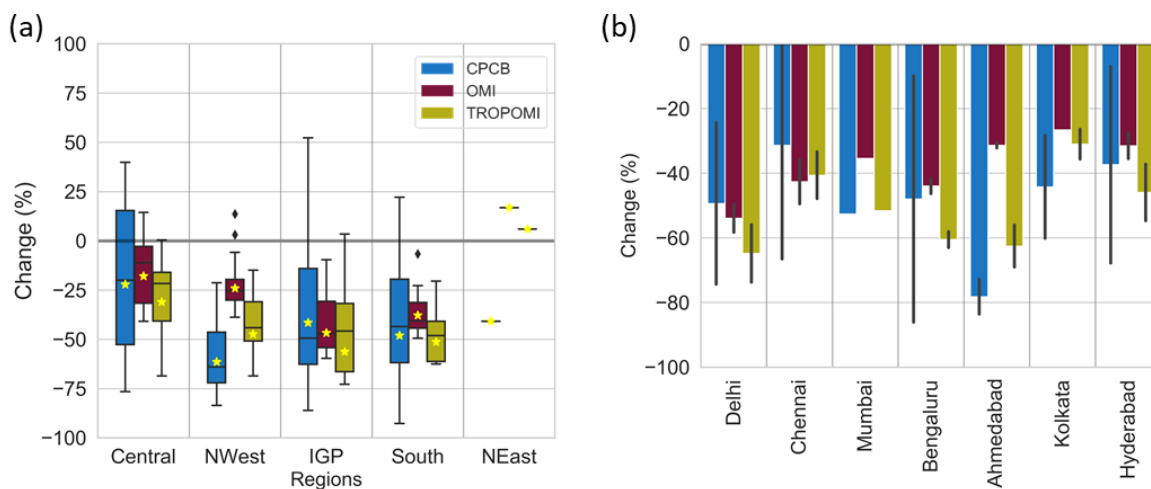
434 Fig. 7(a,b) shows the relationship of OMI and TROPOMI NO₂ with surface NO₂ for the BAU
435 and LDN periods, respectively. During BAU, there are reasonable positive correlations
436 between the satellite instruments and the surface sites (OMI: 0.48, 95 % CI 0.33 - 0.60) and
437 TROPOMI: 0.52, 95 % CI 0.37 - 0.64). In LDN, these correlations drop to 0.36 (95 % CI 0.20
438 - 0.49) and 0.28 (95 % CI 0.12 - 0.43), respectively. The decrease in the correlation during
439 LDN could be due to the decrease in the signal to noise ratio, potentially linked with the primary
440 reduction in urban NO₂ levels. We also determined the correlation between satellite and
441 surface-observed changes during the lockdown (Fig. 7c), finding values of 0.44 (95 % CI 0.28
442 - 0.57) for OMI and 0.49 (95 % CI 0.33 - 0.63) for TROPOMI. This indicates that the lockdown
443 NO₂ reductions appear to be present in both measurement types, providing us with confidence
444 in the observed changes detected in this study. The correlation observed over India in this study
445 is lower than that reported for the USA (Lamsal et al., 2015). The low correlation between OMI
446 and surface NO₂ has been reported earlier by Ghude et al. (2011). While they report the
447 temporal correlation for a single site, our study reports the spatial correlation representing the
448 satellites' ability to capture the spatial heterogeneity. One of the reasons for the lower
449 correlation can be the choice of surface station. Generally, urban background sites are preferred
450 for this kind of analysis. However, the surface NO₂ monitoring station type classification is not
451 available for the CPCB sites. Therefore sites used in the analysis could be potentially impacted
452 by traffic emissions resulting in lower correlation. Another reason is that in-situ measurements
453 are more sensitive to the local emission sources than remotely sensed measurements, and
454 therefore have larger variability resulting in low correlation. Proper classification of the
455 monitoring stations could provide a better assessment of satellite-based observations.

456



457
 458 **Fig. 7 Scatterplots between surface and satellite observed NO₂ for (a) business as usual (BAU)**
 459 **and (b) lockdown (LDN). Panel (c) shows a scatterplot of observed absolute change (LDN-**
 460 **BAU) in surface and satellite NO₂. The values shown in the brackets are the correlation**
 461 **coefficients with 95 % confidence intervals (CI).**

462
 463 The LDN NO₂ percentage change, observed by surface and spatially co-located satellite
 464 measurements, is shown in Fig. 8a for various Indian regions. For this comparison, the number
 465 of available CPCB surface monitoring stations were 17, 15, 81, 25, and 1 for central, north-
 466 west, IGP, south and north-east regions (north region data not available), respectively. Most of
 467 the CPCB stations are in urban areas, so our results reflect changes in predominantly urban-
 468 sourced NO₂. At all surface sites in all regions, there was a percentage reduction greater than
 469 20 % (Fig. 8a). Satellite observations show a similar trend except for the north-east region,
 470 where enhancements are due to forest fires. Both OMI and TROPOMI observed the highest
 471 reduction (~50 %) over IGP. A smaller average reduction of ~20 % over central India might
 472 be due to the aggregate effect of power plants, forest fires and prevalent biomass burning
 473 activities during this season. While the effect of forest fires can be observed in the column NO₂,
 474 its impact on the surface NO₂ is minimal. For the central, IGP and south regions, the mean
 475 percentage change observed by the surface monitoring station is comparable to that observed
 476 by the satellites.



478

479 *Fig. 8 (a) Boxplot showing the percentage change between LDN and BAU in NO₂ levels*
 480 *observed by ground and satellite measurements at CPCB monitoring locations in different*
 481 *regions. (b) Bar chart showing the percentage change in NO₂ levels observed at megacities in*
 482 *India for the same measurements as panel (a). The vertical line in the bar chart is the standard*
 483 *deviation.*

484

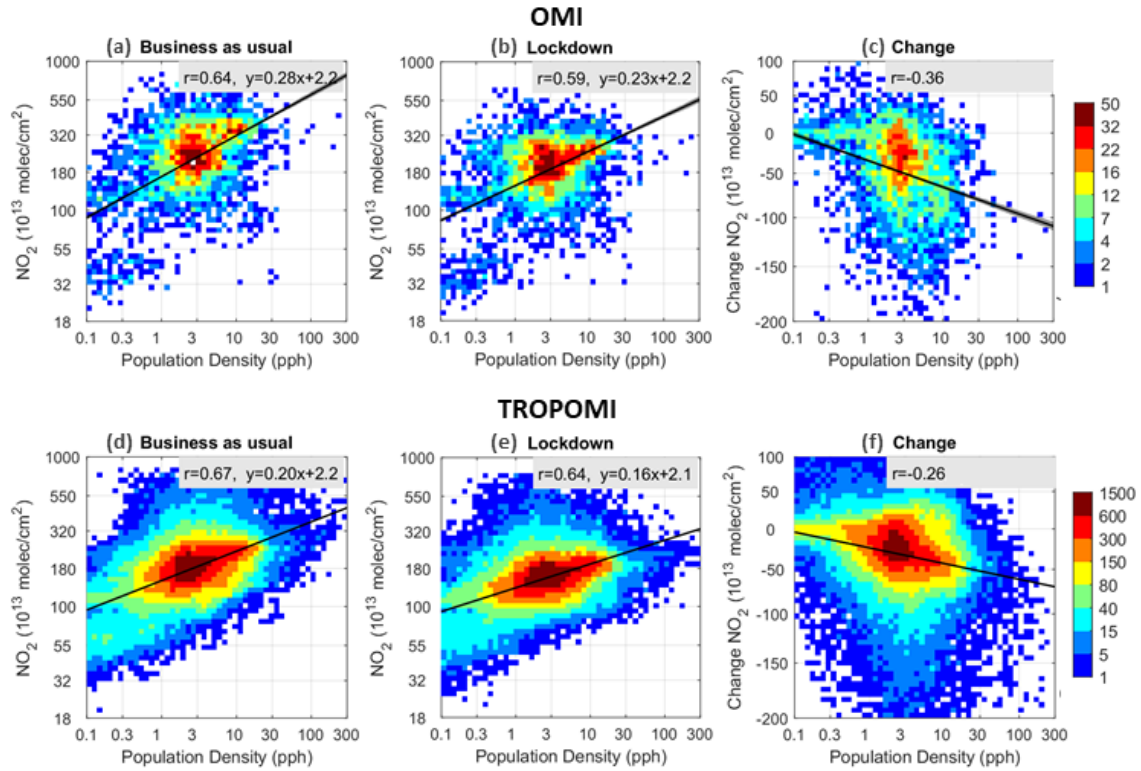
485 We have intercompared the percentage change in NO₂ observed at the surface and satellite over
 486 the major Indian cities (i.e., New Delhi, Chennai, Mumbai, Bangalore, Ahmedabad, Kolkata,
 487 and Hyderabad, Fig. 8b). A significant reduction in the range of ~25-75 % is observed,
 488 consistent in all observational sources used in this study. A similar reduction observed by the
 489 satellites over the cities in other parts of the world has been reported (Tobías et al., 2020;
 490 Naeger and Murphy, 2020; Kanniah et al., 2020; Huang and Sun, 2020). The satellites observe
 491 the largest reduction over Delhi and the smallest over Kolkata. While the observed decline is
 492 comparable for cities, Ahmedabad and Kolkata showed smaller declines than observed by
 493 ground measurements. Also, the reduction observed at the surface has a larger spatial
 494 variability than the one observed from the space. This is potentially linked to the influence of
 495 the local emissions which could not be detected by the space-based instruments because of
 496 relatively large satellite footprints. The results of percentage change observed by OMI are
 497 consistent with the change reported by Pathakoti et al. (2020), although Siddiqui et al. (2020)
 498 reported a higher decline of NO₂ using TROPOMI. This is because we computed the changes
 499 between lockdown and BAU during the same period of the year, whereas Siddiqui et al. (2020)
 500 estimated the changes between the pre-lockdown NO₂ and the lockdown NO₂, which includes
 501 the seasonal component of NO₂. We have also analysed the changes in VCD_{trop} NO₂ observed

502 by both OMI and TROPOMI for the other major cities (Guttikunda et al., 2019), as shown in
503 Fig. S4. A reduction of over 20 % was observed in most cities except for a few in the north-
504 east and central India. Cities showing enhancement or smaller reductions reflect the enhanced
505 fire activities in the north-east and central Indian regions. TROPOMI can capture the reduction
506 over the cities near the fire-prone areas (e.g., Indore and Bhopal) because of its higher spatial
507 resolution.

508

509 **3.7 Correlation of tropospheric columnar NO₂ with the population density**

510 In this section, we examine the VCD_{trop} NO₂ and population relationship for India except where
511 fire anomalies or large thermal power plants existed. The scatter density plots between VCD_{trop}
512 NO₂ and population density for the BAU and LDN analysis period are shown in Fig. 9 for OMI
513 and TROPOMI. The data were log-transformed to establish the log-log relationship as **neither**
514 **dataset is** normally distributed. As the observed changes had negative values, this log
515 transformation was obtained by adding a constant value (Ekwaru and Veugelers, 2018), which
516 was later subtracted when plotting to display the corresponding NO₂ values. Both OMI and
517 TROPOMI NO₂ show a similar relationship with the population density with correlations of ~
518 0.65 during the LDN and BAU periods, suggesting a strong dependence upon the population
519 (i.e., anthropogenic emissions). The slopes of the lines in Fig. 9 (a,b,d,e) show that VCD_{trop}
520 NO₂ follows a power-law scaling with population density (Lamsal et al., 2013). During BAU,
521 the VCD_{trop} NO₂ observed over a grid increased by factors of $10^{0.28} = 1.9$ and $10^{0.20} = 1.58$ for
522 OMI and TROPOMI, respectively, with a ten-fold increase in the population density. The rate
523 of increase of the VCD_{trop} NO₂ during LDN was $10^{0.23} = 1.7$ and $10^{0.16} = 1.45$ times for OMI
524 and TROPOMI, respectively, which was lower than BAU. The correlation during the LDN
525 period was marginally lower than the BAU period. This could be due to a larger reduction in
526 the NO₂ levels in the densely populated grids. The changes observed in the VCD_{trop} NO₂ during
527 the LDN (Fig. 9c & f) were negatively correlated (i.e., reduction was positively correlated)
528 with the population density. The linear relation suggests an increase in the reduction with an
529 increase in the population density; however, some grids exhibit enhancements in VCD_{trop} NO₂
530 due to the local emissions.



531

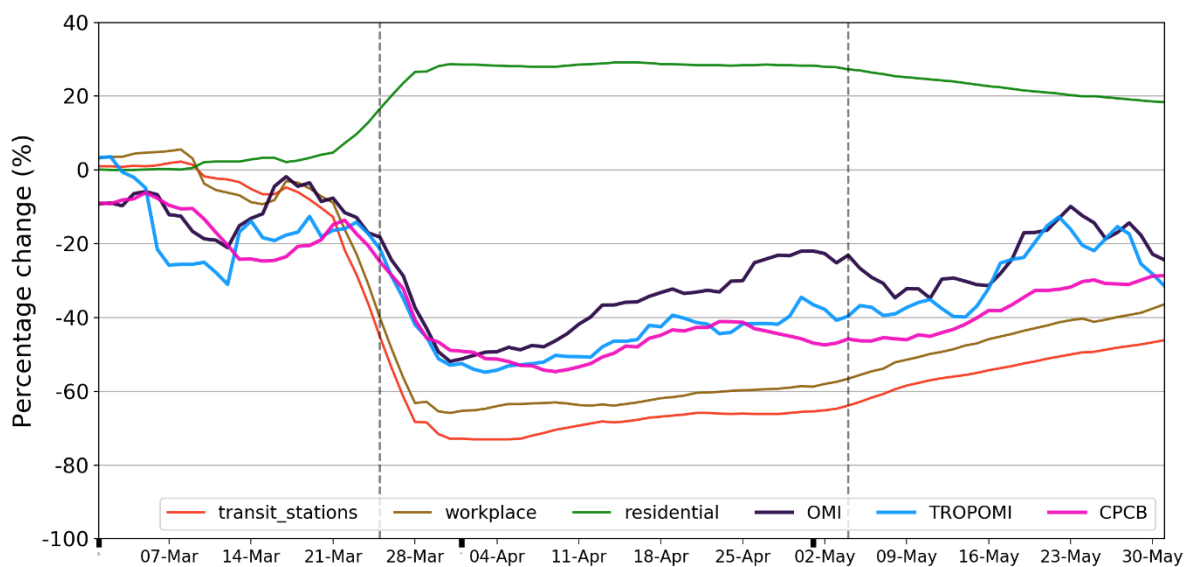
532

533 *Fig. 9. Scatter density plot between the $VCD_{trop} NO_2$ ($\times 10^{13}$ molecules cm^{-2}) and population*
 534 *density (pph) for the analysis period in different years. (a) Business as usual (BAU, 2016–2019)*
 535 *observed by OMI; (b) lockdown (LDN, 2020) observed by OMI; (c) changes (LDN-BAU)*
 536 *observed by OMI; (d) BAU (2019) observed by TROPOMI; (e) LDN (2020) observed by*
 537 *TROPOMI; (f) LND-BAU changes observed by TROPOMI. The linear best fit lines show the*
 538 *log-log relationship between $VCD_{trop} NO_2$ (Y) and population density (X) given by equation $y=$*
 539 *$\beta \cdot x + c$, where $y = \log(Y)$, $x = \log(X)$ and $c = \log(C)$. Therefore, the equation can be written as*
 540 *$\log(Y) = \beta \cdot \log(X) + \log(C)$ or $Y = C \cdot X^\beta$ where β is the slope of the line.*

541 **3.8 Linking the mobility change with NO₂ change**

542 In order to link the observed reduction in NO₂ levels with the traffic emissions over the urban
 543 areas, Fig. 10 shows the seven-day moving average of the daily percentage change observed
 544 by OMI, TROPOMI and CPCB across urban India from 1st March 2020 to 31st May 2020
 545 against the Google mobility percentage reduction for three mobility categories: transit stations,
 546 workplace and residential. Transit stations and workplace, proxies for traffic emissions (Forster
 547 et al., 2020), show a sharp decline (~70 %) due to the lockdown. The signatures of reduced
 548 traffic can be seen even before the start of lockdown in mid March 2020. The decrease in the
 549 workplaces resulted in the enhancement (25-30 %) of the people at a residential location. The
 550 percentage reduction observed by satellites and surface monitoring are consistent with each
 551 other and follow the same trend of the workplaces and transit stations. The reductions observed

552 by satellites and surface monitoring are ~ 20 % lower than the reductions in workplaces and
 553 transit stations which are compensated by the enhancement in residential emissions. Surface
 554 (CPCB) measurements exhibit higher correlation (~ 0.9 and 0.8, with and without moving
 555 average) with the mobility reduction compared to the satellite observation, which has a
 556 relatively weaker correlation (~ 0.8 and 0.5). The positive correlation of NO₂ reduction with
 557 workplaces and transit stations suggests that the reduction observed over the urban areas was
 558 linked with reduced traffic emissions due to travel restrictions for COVID containment.
 559 Moreover, the mobility reduction was higher for larger cities as compared to the smaller ones
 560 (Fig. S6).



561

562 *Fig. 10 Temporal evolution of estimated change (seven-day rolling mean) of satellite*
 563 *observed VCDtrop NO₂ and surface measured NO₂ for the period (March 1st - May 31st,*
 564 *2020) from the baseline.*

565

566 **3.9 Limitations of this study**

567 This study has few limitations that need to be considered while interpreting the results. The
 568 observed changes in the NO₂ levels are the combined effect of changes in the emissions, local
 569 meteorology, large-scale dynamics, and non-linear chemistry. The variability in NO₂, caused
 570 by weather patterns and non-linear chemistry is not included in the present work. Our study
 571 does not distinguish the differences in the upwind and downwind transport of plumes
 572 originating from urban areas and thermal power plants. Moreover, the estimates can be biased
 573 by the forest-fire plumes, which can be transported over a long distance. These limitations
 574 warrant a detailed modelling study to quantify the impact of long-range transport of plumes in

575 the drastic reduction of urban emissions. One of the limitations arises due to the unavailability
576 of the surface monitoring classification according to its location and vicinity of the local
577 sources, which restricted a proper assessment of the space-based NO₂ observation. To
578 overcome this limitation, proper classification of the monitoring stations (Geiger et al., 2013)
579 based on the environment type and vicinity of the sources will be helpful in air quality
580 assesment.

581

582 **4 Conclusions and discussion**

583 The changes in NO₂ levels over India during the COVID-19 lockdown (25th March-3rd May
584 2020) have been studied using satellite-based VCD_{trop} NO₂ observed by OMI and TROPOMI,
585 and surface NO₂ concentrations obtained from CPCB. The changes between lockdown (LDN)
586 and the same period during business as usual (BAU) years have been estimated over different
587 land-use categories (e.g., urban, cropland, and forestland) across six geographical regions of
588 India. Also, the changes observed from space and at the surface have been inter-compared and
589 the correlation with the population density has been studied.

590 Overall, a significant reduction in NO₂ levels of up to ~70 % was observed over India during
591 the lockdown compared to the same period during BAU. The usual prominent NO₂ hotspots
592 observed by OMI and TROPOMI over urban agglomerations during BAU were barely
593 noticeable during the lockdown. However, despite the reduction in electricity production, the
594 coal-based thermal power plants continued to be major NO₂ hotspots during the lockdown.
595 Some of the largest reductions in NO₂ were observed to be over the urban areas of the IGP
596 region. The reduction observed for urban agglomerations was over 150×10^{13} molecules cm⁻²
597 (~30 %) and even more for megacities showing a reduction of around 250×10^{13} molecules cm⁻²
598 (50 %). The reduction observed over the urban areas was linked with reduced traffic emissions
599 due to travel restrictions for COVID containment. The decrease was also observed over rural
600 regions. Average declines of NO₂ in the ranges of 14-30 %, 8-28 % and 10-24 % were observed
601 by OMI and 22-27 %, 6-18 % and 3-21 % were observed by TROPOMI over the urban,
602 cropland and forestland, respectively, in different regions of India. In contrast, an average
603 enhancement over north-east India was observed due to positive fire anomalies during the
604 lockdown. Although we have considered the grids with zero fire anomaly during the lockdown,
605 the fire emissions can still enhance NO₂ levels over grids with no fire activity because of
606 horizontal transport.

607 The observed changes in $VCD_{trop} NO_2$ were found to be spatially positively correlated with
608 surface NO_2 concentrations indicating that the lockdown NO_2 changes appear to be present in
609 both measurement types. The TROPOMI NO_2 showed a better correlation with surface NO_2
610 and was more sensitive to the changes than the OMI because of the finer resolution. Therefore,
611 TROPOMI can provide a better estimate of NO_2 associated with fine-scale heterogeneous
612 emissions. Also, $VCD_{trop} NO_2$ was found to exhibit a good correlation with the population
613 density, suggesting a strong dependence upon the population and hence the anthropogenic
614 emissions. The changes observed in the $VCD_{trop} NO_2$ during the lockdown were negatively
615 correlated (i.e., reduction was positively correlated) with the population density suggesting a
616 larger reduction for the densely populated cities. However, the influence of local emissions can
617 be different in different cities.

618 The analysis presented in this work shows a significant change in NO_2 levels across India. The
619 observed reductions can be linked with the control measures taken to prevent the spread of the
620 COVID-19 that restricted the **people's movement**, resulting in a significant reduction in
621 anthropogenic emissions. As an important message to policymakers, this study indicates the
622 level of **decrease** in NO_2 that is possible if dramatic reductions in key emission sectors such as
623 road traffic were incorporated into air quality management strategies.

624 **5 Data availability.**

625 **OMI data is available at NASA Goddard Earth Sciences Data and Information Services Center**
626 **(GESDISC) (https://disc.gsfc.nasa.gov/datasets/OMNO2d_003/summary).** TROPOMI data is
627 **obtained from (<http://www.temis.nl/airpollution/no2.php>).** Surface measured NO_2 data across
628 India are available at CPCB site (<https://app.cpcbcr.com/ccr/>). VIIRS fire count data is
629 available at FIRMS web portal (<https://firms.modaps.eosdis.nasa.gov/>). India Population data
630 used in this study is available at the <https://www.worldpop.org/>. The LULC data for India is
631 available at the Bhuvan, (<https://bhuvan.nrsc.gov.in/>) Indian Geo-Platform of Indian Space
632 Research Organisation. **ERA5 meteorology is available at CDC**
633 **(<https://cds.climate.copernicus.eu/cdsapp>).** The mobility data is available on Google platform
634 **(<https://www.google.com/covid19/mobility>).**

635 **6 Author contribution**

636 **Akash Biswal and Vikas Singh:** Conceptualization, investigation, visualization, formal
637 analysis, writing original draft, writing, reviewing and editing; **Shweta Singh:** Investigation,

638 writing original draft, discussion, reviewing and editing, **Amit Kesarkar, Ravindra Khaiwal,**
639 **Ranjeet Sokhi, Martyn Chipperfield, Sandip Dhomse, Richard Pope, Tanbir Singh,**
640 **Suman Mor:** Investigation, discussion, reviewing and editing.

641 **7 Declaration of competing interest**

642 The authors declare that they have no known competing financial interests or personal
643 relationships that could have appeared to influence the work reported in this paper.

644 **8 Acknowledgments**

645 The authors are thankful to the Director, National Atmospheric Research Laboratory (NARL,
646 India), for encouragement to conduct this research and provide the necessary support. AB and
647 SS greatly acknowledge the Ministry of Earth Sciences (MoES, India) for the research
648 fellowship. We acknowledge and thank Central Pollution Control Board (CPCB), Ministry of
649 Environment, Forest and Climate Change (MoEFCC, India) for making available air quality
650 data in public. We acknowledge Bhuvan, Indian Geo-Platform of Indian Space Research
651 Organisation (ISRO), National Remote Sensing Centre (NRSC), for providing high-resolution
652 LULC data. The authors gratefully acknowledge OMI, TROPOMI and ERA5 science teams
653 for making data publicly available. We also acknowledge the NASA Goddard Earth Sciences
654 Data and Information Services Center, Tropospheric Emission Monitoring Internet Service and
655 Climate Data Store. We also acknowledge Google community mobility data and report. We
656 acknowledge support from the Air Pollution and Human Health for an Indian Megacity project
657 PROMOTE funded by UK NERC and the Indian MOES, Grant reference number
658 NE/P016391/1.

659

660 **References**

661 **Alonso-Blanco, E., Castro, A., Calvo, A. I., Pont, V., Mallet, M., & Fraile, R.: Wildfire smoke**
662 **plumes transport under a subsidence inversion: Climate and health implications in a distant**
663 **urban area. Science of the Total Environment, 619, 988-1002 2018.**

664 **Archer, C. L., Cervone, G., Golbazi, M., Al Fahel, N. and Hultquist, C.: Changes in air quality**
665 **and human mobility in the USA during the COVID-19 pandemic, Bull. Atmospheric Sci.**
666 **Technol., doi:10.1007/s42865-020-00019-0, 2020.**

667 Barré, J., Petetin, H., Colette, A., Guevara, M., Peuch, V.-H., Rouil, L., Engelen, R., Inness,
668 A., Flemming, J., Pérez García-Pando, C., Bowdalo, D., Meleux, F., Geels, C.,
669 Christensen, J. H., Gauss, M., Benedictow, A., Tsyro, S., Friese, E., Struzewska, J.,
670 Kaminski, J. W., Douros, J., Timmermans, R., Robertson, L., Adani, M., Jorba, O., Joly,
671 M., and Kouznetsov, R.: Estimating lockdown induced European NO₂ changes, *Atmos.*
672 *Chem. Phys. Discuss.*, doi:10.5194/acp-2020-995, in review, 2020.

673 Bauwens, M., Compernelle, S., Stavrakou, T., Müller, J.-F., Gent, J. van, Eskes, H., Levelt, P.
674 F., A, R. van der, Veeffkind, J. P., Vlietinck, J., Yu, H. and Zehner, C.: Impact of
675 Coronavirus Outbreak on NO₂ Pollution Assessed Using TROPOMI and OMI
676 Observations, *Geophys. Res. Lett.*, 47(11), e2020GL087978,
677 doi:10.1029/2020GL087978, 2020.

678 Biswal, A., Singh, T., Singh, V., Ravindra, K. and Mor, S.: COVID-19 lockdown and its impact
679 on tropospheric NO₂ concentrations over India using satellite-based data, *Heliyon*, 6(9),
680 doi:10.1016/j.heliyon.2020.e04764, 2020.

681 Boersma, K. F., Eskes, H. J. and Brinksma, E. J.: Error analysis for tropospheric NO₂ retrieval
682 from space, *J. Geophys. Res. Atmospheres*, 109(D4), doi:10.1029/2003JD003962, 2004.

683 Boersma, K. F., Eskes, H. J., Dirksen, R. J., van der A, R. J., Veeffkind, J. P., Stammes, P.,
684 Huijnen, V., Kleipool, Q. L., Sneep, M., Claas, J., Leitão, J., Richter, A., Zhou, Y. and
685 Brunner, D.: An improved tropospheric NO₂ column retrieval algorithm for the Ozone
686 Monitoring Instrument, *Atmospheric Meas. Tech.*, 4(9), 1905–1928, doi:10.5194/amt-4-
687 1905-2011, 2011.

688 Celarier, E. A., Brinksma, E. J., Gleason, J. F., Veeffkind, J. P., Cede, A., Herman, J. R., Ionov,
689 D., Goutail, F., Pommereau, J.-P., Lambert, J.-C., Roozendael, M. van, Pinardi, G.,
690 Wittrock, F., Schönhardt, A., Richter, A., Ibrahim, O. W., Wagner, T., Bojkov, B., Mount,
691 G., Spinei, E., Chen, C. M., Pongetti, T. J., Sander, S. P., Bucsel, E. J., Wenig, M. O.,
692 Swart, D. P. J., Volten, H., Kroon, M. and Levelt, P. F.: Validation of Ozone Monitoring
693 Instrument nitrogen dioxide columns, *J. Geophys. Res. Atmospheres*, 113(D15),
694 doi:10.1029/2007JD008908, 2008.

695 Chan, K. L., Wiegner, M., van Geffen, J., De Smedt, I., Alberti, C., Cheng, Z., Ye, S., and
696 Wenig, M.: MAX-DOAS measurements of tropospheric NO₂ and HCHO in Munich and
697 the comparison to OMI and TROPOMI satellite observations, *Atmos. Meas. Tech.*, 13,
698 4499–4520, doi:10.5194/amt-13-4499-2020, 2020.

699 Curier, R. L., Kranenburg, R., Segers, A. J. S., Timmermans, R. M. A. and Schaap, M.:
700 Synergistic use of OMI NO₂ tropospheric columns and LOTOS–EUROS to evaluate the
701 NO_x emission trends across Europe, *Remote Sens. Environ.*, 149, 58–69,
702 doi:10.1016/j.rse.2014.03.032, 2014.

703 Duncan, B. N., Lamsal, L. N., Thompson, A. M., Yoshida, Y., Lu, Z., Streets, D. G., Hurwitz,
704 M. M. and Pickering, K. E.: A space-based, high-resolution view of notable changes in
705 urban NO_x pollution around the world (2005–2014), *J. Geophys. Res. Atmospheres*,
706 121(2), 976–996, doi:10.1002/2015JD024121, 2016.

707 Dutheil, F., Baker, J. S. and Navel, V.: COVID-19 as a factor influencing air pollution?,
708 *Environ. Pollut.*, 263, 114466, doi:10.1016/j.envpol.2020.114466, 2020.

709 Ekwaru, J.P. and Veugelers, P.J.: The overlooked importance of constants added in log
710 transformation of independent variables with zero values: A proposed approach for
711 determining an optimal constant. *Statistics in Biopharmaceutical Research*, 10(1), pp.26-
712 29, 2018.

713 ESA, Air pollution drops in India following lockdown
714 [https://www.esa.int/Applications/Observing_the_Earth/Copernicus/Sentinel-](https://www.esa.int/Applications/Observing_the_Earth/Copernicus/Sentinel-5P/Air_pollution_drops_in_India_following_lockdown)
715 [5P/Air_pollution_drops_in_India_following_lockdown](https://www.esa.int/Applications/Observing_the_Earth/Copernicus/Sentinel-5P/Air_pollution_drops_in_India_following_lockdown), 2020. (Accessed: Oct 01, 2020)

716 Eskes, H., van Geffen, J., Boersma, F., Eichmann, K.-U., Apituley, A., Pedergnana, M., Sneep,
717 M., Veefkind, J. P., and Loyola, D.: Sentinel-5 precursor/TROPOMI Level 2 Product User
718 Manual Nitrogen dioxide, Tech. Rep. S5P-KNMI-L2- 0021-MA, Koninklijk Nederlands
719 Meteorologisch Instituut (KNMI),
720 [https://sentinel.esa.int/documents/247904/2474726/Sentinel-5P-Level-2-Product-User-](https://sentinel.esa.int/documents/247904/2474726/Sentinel-5P-Level-2-Product-User-Manual-Nitrogen-Dioxide)
721 [Manual-Nitrogen-Dioxide](https://sentinel.esa.int/documents/247904/2474726/Sentinel-5P-Level-2-Product-User-Manual-Nitrogen-Dioxide), CI-7570-PUM, issue 3.0.0, 2019.

722 Forster, P. M., Forster, H. I., Evans, M. J., Gidden, M. J., Jones, C. D., Keller, C. A., Lamboll,
723 R. D., Quéré, C. L., Rogelj, J., Rosen, D., Schleussner, C.-F., Richardson, T. B., Smith, C.
724 J. and Turnock, S. T.: Current and future global climate impacts resulting from COVID-
725 19, *Nat. Clim. Change*, 10(10), 913–919, doi:10.1038/s41558-020-0883-0, 2020.

726 Gama, C., Relvas, H., Lopes, M. and Monteiro, A.: The impact of COVID-19 on air quality
727 levels in Portugal: A way to assess traffic contribution, *Environ. Res.*, 110515,
728 doi:10.1016/j.envres.2020.110515, 2020.

729 Geiger, J., Malherbe, L., Mathe, F., Ross-Jones, M., Sjoberg, K., Spangl, W., Stacey, B., Ortiz,
730 A.G., de Leeuw, F., Borowiak, A., Galmarini, S., Gerboles, M. and de Saeger,
731 E.: Assessment on siting criteria, classification and representativeness of air quality

732 monitoring stations. JRC–AQUILA Position Paper, 2013
733 <https://ec.europa.eu/environment/air/pdf/SCREAM%20final.pdf>

734 Georgoulias, A. K., van der A, R. J., Stammes, P., Boersma, K. F., and Eskes, H. J.: Trends
735 and trend reversal detection in 2 decades of tropospheric NO₂ satellite observations,
736 *Atmos. Chem. Phys.*, 19, 6269–6294, doi:10.5194/acp-19-6269-2019, 2019.

737 Ghude, S. D., Fadnavis, S., Beig, G., Polade, S. D. and A, R. J. van der: Detection of surface
738 emission hot spots, trends, and seasonal cycle from satellite-retrieved NO₂ over India, J.
739 *Geophys. Res. Atmospheres*, 113(D20), doi:10.1029/2007JD009615, 2008.

740 Ghude, S. D., Kulkarni, P. S., Kulkarni, S. H., Fadnavis, S. and A, R. J. V. D.: Temporal
741 variation of urban NO_x concentration in India during the past decade as observed from
742 space, *Int. J. Remote Sens.*, 32(3), 849–861, doi:10.1080/01431161.2010.517797, 2011.

743 Ghude, S. D., Kulkarni, S. H., Jena, C., Pfister, G. G., Beig, G., Fadnavis, S. and A, R. J. van
744 der: Application of satellite observations for identifying regions of dominant sources of
745 nitrogen oxides over the Indian Subcontinent, *J. Geophys. Res. Atmospheres*, 118(2),
746 1075–1089, doi:10.1029/2012JD017811, 2013.

747 Ghude, S. D., Lal, D. M., Beig, G., A, R. van der and Sable, D.: Rain-Induced Soil NO_x
748 Emission From India During the Onset of the Summer Monsoon: A Satellite Perspective,
749 *J. Geophys. Res. Atmospheres*, 115(D16), doi:10.1029/2009JD013367, 2010.

750 Goldberg, D.L., Anenberg, S.C., Griffin, D., McLinden, C.A., Lu, Z. and Streets, D.G.:
751 Disentangling the impact of the COVID-19 lockdowns on urban NO₂ from natural
752 variability. *Geophys. Res. Lett.*, 47(17), p.e2020GL089269, 2020.

753 Google LLC Community Mobility Reports (Google, accessed in December, 2020);
754 <https://www.google.com/covid19/mobility/>, 2020.

755 Guenther, A. B., Jiang, X., Heald, C. L., Sakulyanontvittaya, T., Duhl, T., Emmons, L. K. and
756 Wang, X.: The Model of Emissions of Gases and Aerosols from Nature version 2.1
757 (MEGAN2.1): an extended and updated framework for modeling biogenic emissions,
758 *Geosci. Model Dev.*, 5(6), 1471–1492, doi:10.5194/gmd-5-1471-2012, 2012.

759 Guttikunda, S. K., Nishadh, K. A. and Jawahar, P.: Air pollution knowledge assessments
760 (APnA) for 20 Indian cities, *Urban Clim.*, 27, 124–141, doi:10.1016/j.uclim.2018.11.005,
761 2019.

762 Guevara, M., Jorba, O., Soret, A., Petetin, H., Bowdalo, D., Serradell, K., Tena, C., Denier van
763 der Gon, H., Kuenen, J., Peuch, V.-H., and Pérez García-Pando, C.: Time-resolved

764 emission reductions for atmospheric chemistry modelling in Europe during the COVID-
765 19 lockdowns, *Atmos. Chem. Phys.*, 21, 773–797, doi:10.5194/acp-21-773-2021, 2021.

766 Hama, S. M. L., Kumar, P., Harrison, R. M., Bloss, W. J., Khare, M., Mishra, S., Namdeo, A.,
767 Sokhi, R., Goodman, P. and Sharma, C.: Four-year assessment of ambient particulate
768 matter and trace gases in the Delhi-NCR region of India, *Sustain. Cities Soc.*, 54, 102003,
769 doi:10.1016/j.scs.2019.102003, 2020.

770 Hersbach, H., Bell, B., Berrisford, P., Hirahara, S., Horányi, A., Muñoz-Sabater, J., Nicolas,
771 J., Peubey, C., Radu, R., Schepers, D. and Simmons, A.: The ERA5 global reanalysis.
772 *Quarterly Journal of the Royal Meteorological Society*, 146(730), pp.1999-2049, 2020.

773 Hilboll, A., Richter, A. and Burrows, J. P.: Long-term changes of tropospheric NO₂ over
774 megacities derived from multiple satellite instruments, *Atmospheric Chem. Phys.*, 13(8),
775 4145–4169, doi:10.5194/acp-13-4145-2013, 2013.

776 Hilboll, A., Richter, A. and Burrows, J. P.: NO₂ pollution over India observed from space – the
777 impact of rapid economic growth, and a recent decline, *Atmos. Chem. Phys. Discuss.*, 1–
778 18, doi:10.5194/acp-2017-101, 2017.

779 Huang, G. and Sun, K.: Non-negligible impacts of clean air regulations on the reduction of
780 tropospheric NO₂ over East China during the COVID-19 pandemic observed by OMI and
781 TROPOMI, *Sci. Total Environ.*, 745, 141023, doi:10.1016/j.scitotenv.2020.141023, 2020.

782 ISFR , Indian State of forest Report, <https://.fsi.nic.in>. Accessed on 27.1.2021, 2019.

783 Kanniah, K. D., Kamarul Zaman, N. A. F., Kaskaoutis, D. G. and Latif, M. T.: COVID-19's
784 impact on the atmospheric environment in the Southeast Asia region, *Sci. Total Environ.*,
785 736, 139658, doi:10.1016/j.scitotenv.2020.139658, 2020.

786 Kramer, L. J., Leigh, R. J., Remedios, J. J. and Monks, P. S.: Comparison of OMI and ground-
787 based in situ and MAX-DOAS measurements of tropospheric nitrogen dioxide in an urban
788 area, *J. Geophys. Res. Atmospheres*, 113(D16), doi:10.1029/2007JD009168, 2008.

789 Krotkov, N. A., Lamsal, L. N., Celarier, E. A., Swartz, W. H., Marchenko, S. V., Bucsela, E.
790 J., Chan, K. L., Wenig, M. and Zara, M.: The version 3 OMI NO₂ standard product,
791 *Atmospheric Meas. Tech.*, 10(9), 3133–3149, doi:10.5194/amt-10-3133-2017, 2017.

792 Krotkov, N. A., Lamsal, L. N., Marchenko, S. V., Swartz, W. H.: OMNO2 README
793 Document Data Product Version 4.0, December 2019, Document Version 9.0. 2019
794 [https://acdsc.gesdisc.eosdis.nasa.gov/data/Aura_OMI_Level3/OMNO2d.003/doc/READ](https://acdsc.gesdisc.eosdis.nasa.gov/data/Aura_OMI_Level3/OMNO2d.003/doc/README.OMNO2.pdf)
795 [ME.OMNO2.pdf](https://acdsc.gesdisc.eosdis.nasa.gov/data/Aura_OMI_Level3/OMNO2d.003/doc/README.OMNO2.pdf) (Accessed 22 Jan 2021)

796 Lamsal, L. N., Duncan, B. N., Yoshida, Y., Krotkov, N. A., Pickering, K. E., Streets, D. G. and
797 Lu, Z.: U.S. NO₂ trends (2005–2013): EPA Air Quality System (AQS) data versus

798 improved observations from the Ozone Monitoring Instrument (OMI), *Atmos. Environ.*,
799 110, 130–143, doi:10.1016/j.atmosenv.2015.03.055, 2015.

800 Lamsal, L. N., Martin, R. V., Donkelaar, A. van, Celarier, E. A., Bucsela, E. J., Boersma, K.
801 F., Dirksen, R., Luo, C. and Wang, Y.: Indirect validation of tropospheric nitrogen dioxide
802 retrieved from the OMI satellite instrument: Insight into the seasonal variation of nitrogen
803 oxides at northern midlatitudes, *J. Geophys. Res. Atmospheres*, 115(D5),
804 doi:10.1029/2009JD013351, 2010.

805 Lamsal, L. N., Martin, R. V., Parrish, D. D. and Krotkov, N. A.: Scaling Relationship for NO₂
806 Pollution and Urban Population Size: A Satellite Perspective, *Environ. Sci. Technol.*,
807 47(14), 7855–7861, doi:10.1021/es400744g, 2013.

808 Lamsal, L. N., Krotkov, N. A., Vasilkov, A., Marchenko, S., Qin, W., Yang, E.-S., Fasnacht,
809 Z., Joiner, J., Choi, S., Haffner, D., Swartz, W. H., Fisher, B., and Bucsela, E.: Ozone
810 Monitoring Instrument (OMI) Aura nitrogen dioxide standard product version 4.0 with
811 improved surface and cloud treatments, *Atmos. Meas. Tech.*, 14, 455–479,
812 doi:10.5194/amt-14-455-2021, 2021.

813 Lane, T. E., Donahue, N. M. and Pandis, S. N.: Effect of NO_x on Secondary Organic Aerosol
814 Concentrations, *Environ. Sci. Technol.*, 42(16), 6022–6027, doi:10.1021/es703225a,
815 2008.

816 Li, F., Zhang, X., Kondragunta, S. and Csiszar, I.: Comparison of Fire Radiative Power
817 Estimates From VIIRS and MODIS Observations, *J. Geophys. Res. Atmospheres*, 123(9),
818 4545–4563, doi:10.1029/2017JD027823, 2018.

819 Lin, J.-T., Liu, M.-Y., Xin, J.-Y., Boersma, K. F., Spurr, R., Martin, R. and Zhang, Q.:
820 Influence of aerosols and surface reflectance on satellite NO₂ retrieval: seasonal and
821 spatial characteristics and implications for NO_x emission constraints, *Atmos. Chem.*
822 *Phys.*, 15(19), 11217–11241, doi:10.5194/acp-15-11217-2015, 2015.

823 Liu, F., Page, A., Strode, S. A., Yoshida, Y., Choi, S., Zheng, B., Lamsal, L. N., Li, C., Krotkov,
824 N. A., Eskes, H., A. R. van der, Veeffkind, P., Levelt, P. F., Hauser, O. P. and Joiner, J.:
825 Abrupt decline in tropospheric nitrogen dioxide over China after the outbreak of COVID-
826 19, *Sci. Adv.*, 6(28), eabc2992, doi:10.1126/sciadv.abc2992, 2020.

827 Mahajan, A. S., De Smedt, I., Biswas, M. S., Ghude, S., Fadnavis, S., Roy, C. and van
828 Roozendaal, M.: Inter-annual variations in satellite observations of nitrogen dioxide and
829 formaldehyde over India, *Atmos. Environ.*, 116, 194–201,
830 doi:10.1016/j.atmosenv.2015.06.004, 2015.

831 Mahato, S., Pal, S. and Ghosh, K. G.: Effect of lockdown amid COVID-19 pandemic on air
832 quality of the megacity Delhi, India, *Sci. Total Environ.*, 730, 139086,
833 doi:10.1016/j.scitotenv.2020.139086, 2020.

834 Martin, R. V., Sioris, C. E., Chance, K., Ryerson, T. B., Bertram, T. H., Wooldridge, P. J.,
835 Cohen, R. C., Neuman, J. A., Swanson, A. and Flocke, F. M.: Evaluation of space-based
836 constraints on global nitrogen oxide emissions with regional aircraft measurements over
837 and downwind of eastern North America, *J. Geophys. Res. Atmospheres*, 111(D15),
838 doi:10.1029/2005JD006680, 2006.

839 Mebust, A. K., Russell, A. R., Hudman, R. C., Valin, L. C. and Cohen, R. C.: Characterization
840 of wildfire NO_x emissions using MODIS fire radiative power and OMI tropospheric NO₂
841 columns, *Atmospheric Chem. Phys.*, 11(12), 5839–5851, [https://doi.org/10.5194/acp-11-](https://doi.org/10.5194/acp-11-5839-2011)
842 [5839-2011](https://doi.org/10.5194/acp-11-5839-2011), 2011.

843 MHA, No.40-3/2020-DM-I (A): Government of India, Ministry of Home Affairs
844 https://www.mha.gov.in/sites/default/files/MHA%20order%20dt%2015.04.2020%2C%20with%20Revised%20Consolidated%20Guidelines_compressed%20%283%29.pdf;
845 [http://www.du.ac.in/du/uploads/PR_Consolidated%20Guideline%20of%20MHA_28032020%20\(1\)_1.PDF](http://www.du.ac.in/du/uploads/PR_Consolidated%20Guideline%20of%20MHA_28032020%20(1)_1.PDF);
846 <https://www.mha.gov.in/sites/default/files/MHA%20Order%20Dt.%2015.04.2020%20to%20extend%20Lockdown%20period%20for%202%20weeks%20w.e.f.%2015.04.2020%20with%20new%20guidelines.pdf>, 2020. (Accessed: Oct 01, 2020)

847
848
849
850

851 Mills, I. C., Atkinson, R. W., Kang, S., Walton, H. and Anderson, H. R.: Quantitative
852 systematic review of the associations between short-term exposure to nitrogen dioxide and
853 mortality and hospital admissions, *BMJ Open*, 5(5), e006946, doi:10.1136/bmjopen-2014-
854 006946, 2015.

855 Monks, P. S., Archibald, A. T., Colette, A., Cooper, O., Coyle, M., Derwent, R., Fowler, D.,
856 Granier, C., Law, K. S., Mills, G. E., Stevenson, D. S., Tarasova, O., Thouret, V., von
857 Schneidemesser, E., Sommariva, R., Wild, O. and Williams, M. L.: Tropospheric ozone
858 and its precursors from the urban to the global scale from air quality to short-lived climate
859 forcer, *Atmos. Chem. Phys.*, 15(15), 8889–8973, doi:10.5194/acp-15-8889-2015, 2015.

860 Muhammad, S., Long, X. and Salman, M.: COVID-19 pandemic and environmental pollution:
861 A blessing in disguise?, *Sci. Total Environ.*, 728, 138820,
862 doi:10.1016/j.scitotenv.2020.138820, 2020.

863 Naeger, A. R. and Murphy, K.: Impact of COVID-19 Containment Measures on Air Pollution
864 in California, *Aerosol Air Qual. Res.*, 20(10), 2025–2034, doi:10.4209/aaqr.2020.05.0227,
865 2020.

866 Navinya, C., Patidar, G. and Phuleria, H. C.: Examining Effects of the COVID-19 National
867 Lockdown on Ambient Air Quality across Urban India, *Aerosol Air Qual. Res.*, 20(8),
868 1759–1771, doi:10.4209/aaqr.2020.05.0256, 2020.

869 Nori-Sarma, A., Thimmulappa, R. K., Venkataramana, G. V., Fauzie, A. K., Dey, S. K.,
870 Venkareddy, L. K., Berman, J. D., Lane, K. J., Fong, K. C., Warren, J. L. and Bell, M. L.:
871 Low-cost NO₂ monitoring and predictions of urban exposure using universal kriging and
872 land-use regression modelling in Mysore, India, *Atmos. Environ.*, 226, 117395,
873 doi:10.1016/j.atmosenv.2020.117395, 2020.

874 NRSC, National Remote Sensing Centre, Natural Resources Census, National Land Use and
875 Land Cover Mapping Using Multitemporal AWiFS Data (LULC-AWiFS), Eighth Cycle
876 (2011-12) Indian Space Research Organisation Department of Space, Government of
877 India. <https://bhuvan-app1.nrsc.gov.in/2dresources/thematic/LULC250/1112.pdf>, 2012.
878 (Accessed: Oct 01, 2020)

879 Pathakoti, M., Muppalla, A., Hazra, S., Dangeti, M., Shekhar, R., Jella, S., Mullapudi, S. S.,
880 Andugulapati, P. and Vijayasundaram, U.: An assessment of the impact of a nationwide
881 lockdown on air pollution – a remote sensing perspective over India, *Atmospheric*
882 *Chem. Phys. Discuss.*, 1–16, doi:<https://doi.org/10.5194/acp-2020-621>, 2020.

883 Penn, E. and Holloway, T.: Evaluating current satellite capability to observe diurnal change in
884 nitrogen oxides in preparation for geostationary satellite missions, *Environ. Res. Lett.*,
885 15(3), 034038, doi:10.1088/1748-9326/ab6b36, 2020.

886 Pope, R. J., Arnold, S. R., Chipperfield, M. P., Latter, B. G., Siddans, R. and Kerridge, B. J.:
887 Widespread changes in UK air quality observed from space, *Atmospheric Sci. Lett.*, 19(5),
888 e817, <https://doi.org/10.1002/asl.817>, 2018.

889 POSOCO: Power system operation corporation limited, monthly statistical report.
890 <https://posoco.in/reports/monthly-reports/monthly-reports-2020-21/>. Last accessed 15 Jan
891 2021.

892 Prasad, A. K., Singh, R. P. and Kafatos, M.: Influence of coal-based thermal power plants on
893 the spatial–temporal variability of tropospheric NO₂column over India, *Environ. Monit.*
894 *Assess.*, 184(4), 1891–1907, doi:10.1007/s10661-011-2087-6, 2012.

895 Prosperi, P., Bloise, M., Tubiello, F. N., Conchedda, G., Rossi, S., Boschetti, L., Salvatore, M.
896 and Bernoux, M.: New estimates of greenhouse gas emissions from biomass burning and

897 peat fires using MODIS Collection 6 burned areas, *Clim. Change*, 161(3), 415–432,
898 doi:10.1007/s10584-020-02654-0, 2020.

899 Russell, A. R., Valin, L. C. and Cohen, R. C.: Trends in OMI NO₂ observations over the United
900 States: effects of emission control technology and the economic recession, *Atmospheric*
901 *Chem. Phys.*, 12(24), 12197–12209, doi:10.5194/acp-12-12197-2012, 2012.

902 Sahu, L. K., Sheel, V., Pandey, K., Yadav, R., Saxena, P. and Gunthe, S.: Regional biomass
903 burning trends in India: Analysis of satellite fire data, *J. Earth Syst. Sci.*, 124(7), 1377–
904 1387, doi:10.1007/s12040-015-0616-3, 2015.

905 Schroeder, W., Oliva, P., Giglio, L. and Csiszar, I. A.: The New VIIRS 375m active fire
906 detection data product: Algorithm description and initial assessment, *Remote Sens.*
907 *Environ.*, 143, 85–96, doi:10.1016/j.rse.2013.12.008, 2014.

908 Sharma, P., Sharma, P., Jain, S. and Kumar, P.: An integrated statistical approach for evaluating
909 the exceedence of criteria pollutants in the ambient air of megacity Delhi, *Atmos. Environ.*,
910 70, 7–17, doi:10.1016/j.atmosenv.2013.01.004, 2013.

911 Sharma, S., Zhang, M., Anshika, Gao, J., Zhang, H. and Kota, S. H.: Effect of restricted
912 emissions during COVID-19 on air quality in India, *Sci. Total Environ.*, 728, 138878,
913 doi:10.1016/j.scitotenv.2020.138878, 2020.

914 Siddiqui, A., Halder, S., Chauhan, P. and Kumar, P.: COVID-19 Pandemic and City-Level
915 Nitrogen Dioxide (NO₂) Reduction for Urban Centres of India, *J. Indian Soc. Remote*
916 *Sens.*, 48(7), 999–1006, doi:10.1007/s12524-020-01130-7, 2020.

917 Shi, Z., Song, C., Liu, B., Lu, G., Xu, J., Vu, T. V., Elliott, R. J. R., Li, W., Bloss, W. J. and
918 Harrison, R. M.: Abrupt but smaller than expected changes in surface air quality
919 attributable to COVID-19 lockdowns, *Sci. Adv.*, 7(3), eabd6696,
920 <https://doi.org/10.1126/sciadv.abd6696>, 2021. Siddiqui, A., Halder, S., Chauhan, P. and
921 Kumar, P.: COVID-19 Pandemic and City-Level Nitrogen Dioxide (NO₂) Reduction for
922 Urban Centres of India, *J. Indian Soc. Remote Sens.*, 48(7), 999–1006,
923 doi:10.1007/s12524-020-01130-7, 2020.

924 Singh, V., Singh, S., Biswal, A., Kesarkar, A. P., Mor, S. and Ravindra, K.: Diurnal and
925 temporal changes in air pollution during COVID-19 strict lockdown over different regions
926 of India, *Environ. Pollut.*, 266, 115368, doi:10.1016/j.envpol.2020.115368, 2020.

927 Solomon, S., Qin, D., Manning, M., Marquis, M., Averyt, K., Tignor, M. M. B., LeRoy Miller,
928 H. J., and Chen, Z.: *Climate Change 2007: 10 Working Group I: The Physical Science*
929 *Basis*, Tech. rep., Intergovernmental Panel on Climate Change, Geneva, 2007.

930 Stevens, F. R., Gaughan, A. E., Linard, C. and Tatem, A. J.: Disaggregating Census Data for
931 Population Mapping Using Random Forests with Remotely-Sensed and Ancillary Data,
932 PLOS ONE, 10(2), e0107042, doi:10.1371/journal.pone.0107042, 2015.

933 Tobías, A., Carnerero, C., Reche, C., Massagué, J., Via, M., Minguillón, M. C., Alastuey, A.
934 and Querol, X.: Changes in air quality during the lockdown in Barcelona (Spain) one
935 month into the SARS-CoV-2 epidemic, *Sci. Total Environ.*, 726, 138540,
936 doi:10.1016/j.scitotenv.2020.138540, 2020.

937 ul-Haq, Z., Tariq, S., Ali, M., Rana, A. D. and Mahmood, K.: Satellite-sensed tropospheric
938 NO₂ patterns and anomalies over Indus, Ganges, Brahmaputra, and Meghna river basins,
939 *Int. J. Remote Sens.*, 38(5), 1423–1450, doi:10.1080/01431161.2017.1283071, 2017.

940 USEPA, CATC.: Nitrogen oxides (NO_x) why and how they are controlled. Diane Publishing.
941 <https://www3.epa.gov/ttnecat1/dir1/fnoxdoc.pdf>, 1999.

942 van der A, R. J., Eskes, H. J., Boersma, K. F., Noije, T. P. C. van, Roozendael, M. V., Smedt,
943 I. D., Peters, D. H. M. U. and Meijer, E. W.: Trends, seasonal variability and dominant
944 NO_x source derived from a ten year record of NO₂ measured from space, *J. Geophys. Res.*
945 *Atmospheres*, 113(D4), doi:10.1029/2007JD009021, 2008.

946 van Geffen, J. H. G. M., Eskes, H. J., Boersma, K. F., Maasakkers, J. D., and Veefkind, J. P.:
947 TROPOMI ATBD of the total and tropospheric NO₂ data products, Report S5P-KNMI-
948 L2-0005-RP, version 2.1.0, to be released, KNMI, De Bilt, the Netherlands, available at:
949 <http://www.tropomi.eu/documents/atbd/> (last access: 10 September 2020), 2019.

950 van Geffen, J., Boersma, K. F., Eskes, H., Sneep, M., ter Linden, M., Zara, M. and Veefkind,
951 J. P.: S5P TROPOMI NO₂ slant column retrieval: method, stability, uncertainties and
952 comparisons with OMI, *Atmos. Meas. Tech.*, 13(3), 1315–1335, doi:10.5194/amt-13-
953 1315-2020, 2020.

954 Veefkind, J. P., Aben, I., McMullan, K., Förster, H., de Vries, J., Otter, G., Claas, J., Eskes, H.
955 J., de Haan, J. F., Kleipool, Q., van Weele, M., Hasekamp, O., Hoogeveen, R., Landgraf,
956 J., Snel, R., Tol, P., Ingmann, P., Voors, R., Kruizinga, B., Vink, R., Visser, H. and Levelt,
957 P. F.: TROPOMI on the ESA Sentinel-5 Precursor: A GMES mission for global
958 observations of the atmospheric composition for climate, air quality and ozone layer
959 applications, *Remote Sens. Environ.*, 120, 70–83, doi:10.1016/j.rse.2011.09.027, 2012.

960 Venkataraman, C., Habib, G., Kadamba, D., Shrivastava, M., Leon, J.-F., Crouzille, B.,
961 Boucher, O. and Streets, D. G.: Emissions from open biomass burning in India: Integrating
962 the inventory approach with high-resolution Moderate Resolution Imaging

963 Spectroradiometer (MODIS) active-fire and land cover data, *Glob. Biogeochem. Cycles*,
964 20(2), doi:10.1029/2005GB002547, 2006.

965 Venter, Z. S., Aunan, K., Chowdhury, S. and Lelieveld, J.: COVID-19 lockdowns cause global
966 air pollution declines, *Proc. Natl. Acad. Sci.*, 117(32), 18984–18990,
967 doi:10.1073/pnas.2006853117, 2020.

968 Wang, C., Wang, T., Wang, P. and Rakin, V.: Comparison and Validation of TROPOMI and
969 OMI NO₂ Observations over China, *Atmosphere*, 11(6), 636,
970 doi:10.3390/atmos11060636, 2020.

971 WorldPop.: India 100m Population, Version 2. University of Southampton. DOI:
972 10.5258/SOTON/WP00532 2017, 2017.

973 Yarragunta, Y., Srivastava, S., Mitra, D. and Chandola, H. C.: Influence of forest fire episodes
974 on the distribution of gaseous air pollutants over Uttarakhand, India, *GIScience Remote*
975 *Sens.*, 57(2), 190–206, <https://doi.org/10.1080/15481603.2020.1712100>, 2020.